Lifelong restriction of dietary valine has sex-specific benefits for health and lifespan in mice

Mariah F. Calubag[1,2,3], Ismail Ademi[1,2], Cara L. Green[1,2], Hashan S. M. Jayarathne[4,5], Dulmalika N.H. Manchanayake[4,5], Sandra M. Le[1,2], Penelope Lialios[1,2], Lucia E. Breuer[1,2], Shoshana Yakar[6], Reji Babygirija[1,2,3], Michelle M. Sonsalla[1,2], Isaac Grunow[1,2], Chung-Yang Yeh[1,2], Yang Liu[1,2,7], Bailey A. Knopf[1,2,3], William A. Ricke[8,9], Teresa T. Liu[8,10], Mariana Sadagurski[4,5], Dudley W. Lamming[1,2,3,7,9,11,12*]

[1]Department of Medicine, University of Wisconsin-Madison, Madison, WI 53705, USA
[2]William S. Middleton Memorial Veterans Hospital, Madison, WI 53705, USA
[3]Graduate Program in Cellular and Molecular Biology, University of Wisconsin-Madison, Madison, WI 53705, USA
[4]Department of Biological Sciences, Wayne State University, Detroit, MI, USA
[5]Institute of Environmental Health Sciences, Integrative Biosciences Center, Wayne State University, Detroit, MI, USA
[6]New York University College of Dentistry, New York, NY 10010, United States
[7]Comparative Biomedical Sciences Graduate Program, University of Wisconsin-Madison, Madison, WI, USA
[8]George M. O'Brien Center of Research Excellence, Department of Urology, University of Wisconsin, Madison, WI 93705, USA
[9]Wisconsin Nathan Shock Center of Excellence in the Basic Biology of Aging, Madison, WI 53705, USA
[10]Department of Pharmaceutical Sciences, St. John Fisher University, Rochester, NY 14618, USA
[11]University of Wisconsin-Madison Comprehensive Diabetes Center, Madison, WI 53705, USA
[12]University of Wisconsin Carbone Comprehensive Cancer Center, Madison, WI 53705, USA

***Correspondence and Lead Contact**
Dudley W. Lamming, PhD
Associate Professor of Medicine
University of Wisconsin-Madison
1685 Highland Ave
MFCB Rm 4147
Madison, WI 53705, USA
dlamming@medicine.wisc.edu
Tel: 608-262-7341

Abstract

Dietary protein is a key regulator of metabolic health in humans and rodents. Many of the benefits of protein restriction are mediated by reduced consumption of dietary branched-chain amino acids (BCAAs; leucine, valine and isoleucine), and restriction of the BCAAs is sufficient to extend healthspan and lifespan in mice. While the BCAAs have often been considered as a group, it has become apparent that they have distinct metabolic roles, and we recently found that restriction of isoleucine is sufficient to extend the healthspan and lifespan of male and female mice. Here, we test the effect of lifelong restriction of the BCAA valine on healthy aging. We find that valine restriction (Val-R) improves metabolic health in C57BL/6J mice, promoting leanness and glycemic control in both sexes. To investigate the molecular mechanisms engaged by Val-R with aging, we conducted multi-tissue transcriptional profiling and gene network analysis. While Val-R had a significantly greater molecular impact in the liver, muscle, and brown adipose tissue of female mice than males, there was a stronger gene enrichment with phenotypic traits in male mice. Further, we found that phenotypic changes are associated with a multi-tissue downregulation of the longevity associated PI3K-Akt signaling pathway. Val-R reduces frailty in both sexes and extends the lifespan of male by 23%, but does not extend female lifespan, corresponding with a male-specific downregulation of PI3K-Akt signaling. Our results demonstrate that Val-R improves multiple aspects of healthspan in mice of both sexes and extends lifespan in males, suggests that interventions that mimic Val-R may have translational potential for aging and age-related diseases.

Keywords: aging; branched-chain amino acids; frailty; valine; lifespan; metabolic health; mice

Introduction

Dietary interventions have strong effects on health and lifespan, with calorie restriction extending lifespan in diverse species and improving health in humans [1,2]. Recently, it has become clear that interventions that alter dietary levels of specific macronutrients instead of reducing calories can also promote healthy aging. In particular, emerging evidence suggests dietary protein is a key regulator of healthy aging.

Protein has generally been thought of as beneficial for healthy aging, as protein promotes satiety and can be used to promote weight loss [3,4], and increased protein intake is often recommended for the elderly to combat sarcopenia [5]. However, several different retrospective and prospective cohort studies have shown that higher protein consumption is associated with diseases of aging including diabetes [6-9] and sarcopenia [10]. Randomized clinical trials have shown that protein restriction (PR) improves metabolic health, reducing adiposity and improving insulin sensitivity [11-13]. Finally, multiple studies have shown that PR promotes metabolic health and even extends lifespan in flies and mice [14-18].

Many of the benefits of PR may be due to reduced intake of specific essential amino acids. While restriction of several different amino acids has been shown to improve health without reducing calorie intake [19-21], we have focused on the branched-chain amino acids (BCAAs; leucine, isoleucine and valine). Blood levels of BCAAs are specifically reduced in blood by PR in humans [12], and we have found that restriction of the BCAAs improves metabolic health in C57BL/6J mice of both sexes and extends the lifespan of males by over 30% [17]. Isoleucine is the most potent of the BCAAs in its impact on metabolic health. Restriction of isoleucine alone is sufficient to improve overall metabolic health as well as reduce molecular markers of aging in C57BL/6J mice [22,23]. Further, isoleucine restriction extends the lifespan of flies and UM-HET3 mice [24-26].

While each BCAA has been shown to have specific effects on metabolic health, the impact of restricting either leucine or valine on healthy aging and lifespan has not been investigated. While leucine is a potent agonist of mTORC1, an amino acid-sensitive protein kinase that is a central regulator of metabolism and aging [27,28], restriction of leucine in our hands is associated with negligible metabolic benefits, and leucine supplementation has been shown to not significantly impact lifespan [22,29,30]. In contrast, recent work on valine has shown that valine is associated with cancer, inflammation, insulin resistance and glucotoxicity in mice as well as human and porcine cell culture models [31-35]. We have also found that dietary restriction of valine alone can reverse diet-induced obesity and restore glucoregulatory control in C57BL/6J males [22,30].

Here, we investigate the hypothesis that valine restriction (Val-R) increases the healthspan and lifespan of mice. We find that lifelong Val-R improves metabolic health and reduces frailty in C57BL/6J mice of both sexes, and increases the lifespan of male but not female mice when started at one month of age. Val-R also improves the cognition of female mice, which is accompanied by a reduction in neuroinflammatory markers in both sexes. We identify sex-specific molecular effects of Val-R on the transcriptome of multiple tissues. By correlating gene expression with phenotypic traits, we found that male Val-R-fed mice display an overall downregulation of the

PI3K-Akt signaling pathway, a pathway whose downregulation is involved in longevity in multiple organisms and has been shown to be an upstream regulator of mTORC1. Surprisingly, while restriction of valine would be predicted to reduce mTORC1 activity, multiple pathways associated with mTORC1 signaling were increased by Val-R, a finding we confirmed through immunoblotting of mTORC1 substrates. This work suggests that lowering dietary valine should be explored as a potential intervention for age-related diseases and to gain insight into new longevity mechanisms. In conclusion, these results demonstrate the unique role of dietary valine, and expand the universe of dietary components which control healthy aging.

Methods

Animal care, housing and diet

All procedures were performed in conformance with institutional guidelines and were approved by the Institutional Animal Care and Use Committee of the William S. Middleton Memorial Veterans Hospital. Male and female C57BL/6J mice were purchased from The Jackson Laboratory (Bar Harbor, ME, USA) at 3 weeks of age. All mice were acclimated to the animal research facility for one week before entering studies. All animals were housed in static microisolator cages in a specific pathogen-free mouse facility with a 12:12 h light–dark cycle, maintained at approximately 22°C.

Mice were fed amino acid-defined diets with either full valine (TD.140711; CTL) or a 67% restriction of valine (TD.160735; Val-R) (full diet compositions are provided in **Table S1**; Inotiv, Madison, WI, USA). Diets were started at 4 weeks of age and continued lifelong.

Lifespan Study

Mice were randomized into diet groups and enrolled in the survival study at 4 weeks of age. Mice were euthanized for humane reasons if moribund, developed other problems such as excessive tumor burden or upon the recommendation by the facility veterinarian. Mice found dead were noted at daily inspection and saved in the refrigerator. Gross necropsy was performed on euthanized mice and on found dead mice in suitable condition, during which the abdominal and thoracic cavities were examined for the presence of solid tumors, splenomegaly or infection. Based on this inspection, the presence or absence of cancer was noted. A second cohort of mice was sacrificed at 24 months of age for cross-sectional analysis; all mice in this second cohort were also included in the lifespan analysis. Mice were censored as of the date of death if removed for cross-sectional analysis, or if death was due to experimental error. The lifespan of all mice can be found in **Table S5.**

Metabolic Phenotyping

Glucose, insulin and alanine tolerance tests were performed by fasting all mice for 4 hours or overnight (~16 hours) and then injecting either glucose (1g/kg), insulin (0.75U/kg) or pyruvate (2g/kg) intraperitoneally [36,37].

Blood glucose levels were determined at the indicated times using a Bayer Contour blood glucose meter (Bayer, Leverkusen, Germany) and test strips. Body composition was determined using an EchoMRI Body Composition Analyzer. For assay of multiple metabolic parameters (O_2, CO_2, food

consumption, and activity tracking), mice were acclimatized to housing in a Columbus Instruments Oxymax/CLAMS-HC metabolic chamber system for approximately 24 hours, and data from a continuous 24-hour period was then recorded and analyzed.

Physical fitness testing via rotarod and inverted cling assays

To assess motor coordination via a rotarod assay, mice were trained at a constant speed of 4 rpm the day before testing. On the day of testing, mice were put onto the rotarod for three rounds, at least 30 min apart, and the average time spent on the rotarod, and the maximum speed were recorded. During the testing, the rotarod started at a speed of 4 rpm with an acceleration of 0.5 rpm/s up to a maximum of 40 rpm. To assess grip strength via the inverted cling test, mice were placed on a wire frame and carefully inverted until the mice are hanging upside down. The timer then started, and the time until the mouse fell was recorded. The average time of three rounds of testing conducted at least 30 min apart was calculated.

Frailty Index Scoring

Frailty was assessed longitudinally using a 28-item list frailty index whose measures are based on procedures outlined in [38]. This frailty index reflects an accumulation of age-associated deficits similar to the Rockwood frailty index in humans [39]. The items are scored from 0 (no deficit) to 0.5 (mild deficit) to 1 (severe deficit). The scored criteria include alopecia, loss of fur color, dermatitis, loss of whiskers, coat condition, tumors, distended abdomen, kyphosis, tail stiffening, gait disorders, tremor, body condition score, vestibular disturbance, cataracts, corneal opacity, eye discharge/swelling, microphthalmia, vision loss, menace reflex, nasal discharge, malocclusions, rectal prolapse, vaginal/uterine/penile prolapse, diarrhea, breathing rate/depth, mouse grimace score, and piloerection. The scores for all items are averaged to give the frailty score. Complete frailty scores can be found in **Tables S6 and S7**.

Void Spot Assay

Void spot assays were performed as described previously [26,40]. Mice were individually placed in standard mouse cages with thick chromatography paper (Ahlstrom, Kaukauna, WI). During the study period (4 hours), mice were restricted from water. Chromatography papers were imaged with a BioRad ChemiDoc Imaging System (BioRad, Hercules, CA) using an ethidium bromide filter set and 0.5 second exposure to ultraviolet light. Images were imported into ImageJ and total void spots analyzed with VoidWhizzard.

Novel Object Recognition (NOR) assay

A novel object recognition test (NOR) was performed in an open field where the movements of the mouse were recorded using a camera mounted above the field as previously described [41]. Before each test, mice were acclimatized in the behavioral room for at least 30 min and were given a 5 minute habituation trial with no objects on the field. This was followed by a short-term memory test (STM) phase on the same day that consisted of one acquisition trial and a test trial. The next day, we conducted a long-term memory test (LTM) consisting of only a test trial. In the acquisition trial, the mice were allowed to explore two identical objects placed diagonally on opposite sides of the field for 5 minutes. One hour after the acquisition trial, STM was performed, and 24 hours later, LTM was performed. Both test trials were performed by replacing one of the identical objects of the acquisition trial with a novel object. The results were quantified using a

discrimination index (DI), representing the ratio of the duration of exploration for the novel object compared to the old object.

Collection of tissues for molecular and histological analysis

Mice were euthanized in the fed state at 24 months of age, where they were fasted overnight starting the day prior to sacrifice; in the morning, mice were refed for 3 hours and then sacrificed. Following blood collection via submandibular bleeding, mice were euthanized by cervical dislocation and tissues were rapidly collected, weighed, and snap frozen in liquid nitrogen. A portion of the liver was directly embedded into Tissue-Tek Optimal Cutting Temperature (OCT) compound. It was sent to the University of Wisconsin-Madison Carbone Cancer Center Experimental Animal Pathology Laboratory (UWCCC EAPL) for cryosectioning and staining for Oil-red-O (ORO). Another portion of the liver as well as a portion of the kidney and spleen was fixed in 10% formalin for 4 hours, transferred to 30% sucrose for 24 hours and then embedded in OCT and then cryosectioned and stained for SA-β-Gal activity. The inguinal white adipose tissue (iWAT) and brown adipose tissue (BAT) were fixed in 10% formalin for 24 hours, switched to 70% ethanol and then paraffin-embedded before being cryosectioned and stained for Hematoxylin and eosin (HE). Images of the liver, kidney, spleen, iWAT and BAT were taken using an EVOS microscope (Thermo Fisher Scientific Inc., Waltham, MA, USA) at a magnification of 40X as previously described [42,43]. Quantification fields were obtained for each tissue from each mouse and quantified using ImageJ (NIH, Bethesda, MD, USA).

For histological analysis, brains were fixed in 10% formalin for 24 hours and transferred to 30% sucrose. Brains were postfixed, dehydrated, and then sectioned coronally (30 μm) using a sliding microtome, followed by immunofluorescent analysis as described [44]. For immunohistochemistry, brain sections were washed with PBS six times, blocked with 0.3% Triton X-100 and 3% normal donkey serum in PBS for 2 hours before staining was carried out overnight using rabbit anti-GFAP (1:1000; Millipore, Cat. No. ab5804 primary antibody. For goat anti-Iba1 (1:1000 Abcam Cat. No. ab5076), immunostaining brain sections were pretreated with 0.5% NaOH and 0.5% H_2O_2 in PBS for 20 minutes. After the primary antibody brain sections were incubated with AlexaFluor-conjugated secondary antibodies for 2 hours (Invitrogen). Microscopic images of the stained sections were obtained using an Olympus FluoView 500 and Zeiss LSM 800 Laser Scanning Confocal Microscope.

Micro-computed tomography

Right femurs from all animals were collected for micro-computed tomography (μCT). Bones were fixed in 10% formalin and placed on a rocker for 24 hours before being rinsed, placed in 70% ethanol, and stored at 4°C. All bones were scanned using the same instrument under the same conditions, following the American Society for Bone and Mineral Research guidelines [45]. Using a high-resolution SkyScan micro-CT system (SkyScan 1172, Kontich, Belgium) with 10-MP digital detector, 10 W of energy (60 kV and 167 mA), and a pixel size of 9.7 microns, exposure 925 ms/frame rotation step 0.3 degrees with ×10 frame averaging, 0.5-mm aluminum filter (to increase the transmission), samples were scanned in the air with scan rotation of 180 degrees. Before morphometric analysis, global thresholding was applied. Image reconstruction was done using NRecon software (version 1.7.3.0; Bruker micro-CT, Kontich, Belgium). Data analysis was done using CTAn software (version 1.17.7.2+; Bruker micro-CT, Kontich, Belgium). 3D images

were constructed using CT Vox software (version 3.3.0 r1403; Bruker micro-CT, Kontich, Belgium).

Immunoblotting

Tissue samples from liver and muscle were lysed in cold RIPA buffer supplemented with phosphatase inhibitor and protease inhibitor cocktail tablets (Thermo Fisher Scientific, Waltham, MA, USA) as previously described [17,46] using a FastPrep 24 (M.P. Biomedicals, Santa Ana, CA, USA) with screw cap microcentrifuge tubes (822-S) from (Dot Scientific, Burton, MI) and ceramic oxide bulk beads (10158-552) from VWR (Radnor, PA, USA). Protein lysates were then centrifuged at 13,300 rpm for 10 minutes and the supernatant was collected. Protein concentration was determined by Bradford (Pierce Biotechnology, Waltham, MA, USA). 20 µg protein was separated by SDS–PAGE (sodium dodecyl sulfate–polyacrylamide gel electrophoresis) on 16% resolving gels (Thermo Fisher Scientific, Waltham, MA, USA) and transferred to PVDF membrane (EMD Millipore, Burlington, MA, USA). pT389-S6K1 (9234), S6K1 (9202), pS240/244-S6 (2215), S6 (2217), pThr37/46 4E-BP1 (2855), 4E-BP1 (9644), eIF2α (5324), pS51-eIF2α (3597), AMPKa (5831), pAMPKa (4188), Beclin-1 (3495), LC3A/B (12741), GAPDH (2118), and β-tubulin (2146) were purchased from Cell Signaling Technologies (CST, Danvers, MA, USA) and used at a dilution of 1:1000. p62 (American Research Products, #03-GP62-C) was also used at a dilution of 1:1000. Imaging was performed using a Bio-Rad Chemidoc MP imaging station (Bio-Rad, Hercules, CA, USA). Quantification was performed by densitometry using NIH ImageJ software.

Quantitative real-time PCR (qRT-PCR)

qRT-PCR was carried out according to protocols as previously described [42]. using TRI Reagent according to the manufacturer's protocol. The concentration and purity of RNA were determined by absorbance at 260/280 nm using Nanodrop (Thermo Fisher Scientific). 1 µg of RNA was used to generate cDNA (Superscript III; Invitrogen, Carlsbad, CA, USA). Oligo dT primers and primers for real-time PCR were obtained from Integrated DNA Technologies (IDT, Coralville, IA, USA). Reactions were run on an StepOne Plus machine (Applied Biosystems, Foster City, CA, USA) with Sybr Green PCR Master Mix (Invitrogen). Actin was used to normalize the results from gene-specific reactions.

The primers that were used are as follows:

Gene	**Sequences**
Actb	Fwd 5'-GATGTATGAAGGCTTTGGTC-3' Rev 5'-TGTGCACTTTTATTGGTCTC-3'
Cidea	Fwd 5'-GAATAGCCAGAGTCACCTTCG-3' Rev 5'-AGCAGATTCCTTAACACGGC-3'
Elolv3	Fwd 5'-ATGCAACCCTATGACTTCGAG-3' Rev 5'-ACGATGAGCAACAGATAGACG-3'
Ucp1	Fwd 5'-GCATTCAGAGGCAAATCAGC-3' Rev 5'-GCCACACCTCCAGTCATTAAG-3'

Senescence-Associated B-Galactosidase Staining

Enhanced lysosomal biogenesis, a common feature of cellular senescence, can be detected by measuring β-galactosidase (lysosomal hydrolase) activity at pH 6.0 [47]. This senescence-associated β-galactosidase (SA-β-Gal) activity appears to be restricted to senescent cells at a low pH [48,49]. SA-β-Gal activity is shared by almost all senescent cells, but particular care should be taken when detecting this in cultured cells because high confluency and contact inhibition can increase SA-β-gal activity [48,50]. Fresh tissue from mice was collected and fixed in 10% neutral buffered formalin (NBF) on ice for 3-4 hr. Tissues were then transferred to 30% sucrose at 4°C for 24 hours before being embedded in O.C.T. compound in a cryomold and stored at -80°C. Prior to cryosectioning, tissues were equilibrated at -20°C and then cryosectioned into 5-7 µm sections before being attached to Superfrost Plus slides. Fresh SA-β-Gal staining solution at a pH of 6 was prepared as previously described. Tissue slides were stained in SA-β-Gal staining solution for 18-24 hrs at 37°C in a non-CO2 incubator before being rinsed three times with PBS. To prevent crystal formation a parafilm Coplin jar was used to prevent evaporative loss of staining solution. Stained sections were imaged using the EVOS microscope (Thermo Fisher Scientific Inc., Waltham, MA, USA) at a magnification of 40X as previously described. The percent of SA-βgal-positive area for each sample will be quantified using ImageJ.

ELISA assays and kits

Blood plasma for FGF21 and insulin was obtained at 19 months of age in the fasted state. Blood FGF21 levels were assayed by a mouse/rat FGF-21 quantikine ELISA kit (MF2100) from R&D Systems (Minneapolis, MN, USA). Plasma insulin was quantified using an ultra-sensitive mouse insulin ELISA kit (90080), from Crystal Chem (Elk Grove Village, IL, USA).

Transcriptomics

RNA was extracted from the liver, BAT and muscle using the PureLink RNA mini kit (Invitrogen, 12183025) with DNase (Invitrogen, 12185010) following manufacturer's instructions. The concentration and purity of RNA was determined using a NanoDrop 2000c spectrophotometer (Thermo Fisher Scientific, Waltham, MA) and RNA was diluted to 100–400 ng/mL for sequencing. Total RNA was submitted to the University of Wisconsin-Madison Biotechnology Center Gene Expression Center (RRID:SCR_017757) & DNA Sequencing Facility (RRID:SCR_017759) for RNA quality assessment on an Agilent Biomek Plate Reader (A260/A280) and Agilent 4200Tapestation (RIN). RNA libraries were prepared using the NEBNext® Ultra™ II Directional RNA Library Prep Kit Illumina (New England Biolabs GmbH, Frankfurt, DE) with a 500ng total RNA input. Paired end 150bp sequencing was done on an Illumina NovaSeq X Plus sequencer. Adapter-trimmed strand-specific 2×150 bp Illumina reads were processed with Skewer v0.1.123 (Jiang et al., 2014) to remove sequencing adapters and low-quality bases [51]. Reads were aligned to the *Mus musculus* GRCm39 reference genome (NCBI assembly accession GCA_000001635.9) using STAR v2.7.11b (Dobin et al., 2013) with splice-aware alignment and transcript annotations from Ensembl release 110 [52]. STAR was run with the options --twopassMode Basic to improve splice junction discovery and --outSAMtype BAM SortedByCoordinate to produce coordinate-sorted BAM files suitable for downstream analysis. Expression quantification at the gene and transcript levels was performed with RSEM v1.3.1 (Li and Dewey, 2011) using the STAR-aligned BAM files as input. The RSEM reference was prepared using the corresponding Ensembl transcript annotations [53].

Analysis of significantly differentially expressed genes (DEGs) was completed in R version 4.4.1 using *edgeR* and *limma* packages. Gene names were converted to gene symbol and Entrez ID formats using the *mygene* package. PCA plots were generated using the *mixomics* package. DEGs were used to identify enriched pathways, both Gene Ontology (for Biological Processes) and KEGG enriched pathways using an adjusted p-value cut-off of 0.05 (**Tables S2-S5**). All genes, log2 fold-changes and corresponding unadjusted and Benjamini-Hochberg adjusted p values can be found in **Tables S2-S5**.

WGCNA analysis was conducted in R (Version 4.4.3) using the WGCNA package. We analyzed males and females separately. First, we filtered by gene expression variance, keeping the top 50% variable genes for each tissue to remove "noisy" genes. We combined genes from all three tissues, which were demarcated to indicate their tissue origin. We then checked that all genes had enough samples and there were no clear outliers before running the analysis. We started with 25197 genes for females and 22928 for males. WGCNA analysis identifies significant modules of genes and their correlations with phenotypes. Once modules of genes were identified, they were enriched for KEGG Pathways, we then separated out genes by their original tissue type and re-ran the KEGG enrichment analysis to identify tissue specific pathways that were related to phenotypes of interest.

Statistics

Data are presented as the mean ± SEM unless otherwise specified. Statistical analyses were performed using one-way or two-way ANOVA followed by Tukey–Kramer post hoc test, as specified in the figure legends. Outliers were excluded using the Robust Regression Outlier Test (ROUT) in Graphpad Prism (v10), Q=1%, and are indicated by an asterisk(*) and blue colored font in the Source Data. Lifespan comparisons were calculated by log rank test. Maximum lifespan calculations were made by generating a cutoff of the top 25% longest lived animals in each sex, coupled with Boschloo's Test (Wang-Allison) for significance testing between groups. Healthspan by FAMY (Frailty Adjusted Mouse Years) and GRAIL (Gauging Robust Aging when Increasing Lifespan) were calculated as described [54]. Other statistical details are available in the figure legends. Energy expenditure differences were detected using analysis of covariance (ANCOVA). ANCOVA analysis assumes a linear relationship between the variables and their covariates. If the slope is equal between groups, then the regression lines are parallel, and elevation is then tested to determine any differences (i.e., if slopes are statistically significantly different, elevation will not be determined). In all figures, n represents the number of biologically independent animals. Sample sizes were chosen based on our previously published experimental results with the effects of dietary interventions. Data distribution was assumed to be normal, but this was not formally tested.

Randomization

All studies were performed on animals or on tissues collected from animals. Young animals of each sex were randomized into groups of equivalent weight, housed 3 animals per cage, before the beginning of the *in vivo* studies.

Results

Valine restriction improves the metabolic health of male and female mice

We began our lifespan study by randomizing male and female C57BL/6J mice to one of two amino acid (AA)-defined diets starting at 4 weeks of age and followed them longitudinally (**Fig. 1A**). Briefly, our control (CTL) diet contained all twenty common AAs; the diet composition reflects that of a natural chow in which 21% of calories are derived from protein. We also utilized a diet in which the level of valine was reduced by 67% (valine restricted, Val-R). These diets are isocaloric, with identical levels of fat and carbohydrates; the reduction in valine was balanced by a proportional increase in non-essential AAs, keeping the percentage of calories derived from AAs constant. The full composition of these diets is summarized in **Table S1**.

We measured body weight monthly and assessed body composition every 6 months. Val-R-fed mice of both sexes gained weight more slowly than their CTL-fed counterparts, with a highly significant difference at 24 months of age (**Figs. 1B-D**). The lower weight of Val-R-fed mice was the result of reduced accretion of both lean mass and fat mass; the greater impact on fat mass resulted in an overall reduction in adiposity in both sexes (**Figs. 1E-M**). While Val-R-fed mice were leaner and lighter, with reduced iWAT and eWAT, but increased quadricep muscle mass when corrected to body weight, they did not show decreased linear growth, as tibia and femur length were comparable to controls (**Supplementary Figs. 1A-I, 1D-O**).

We also assessed the effects of Val-R on other aspects of femoral bone morphology using micro-CT. Val-R significantly decreased total cross-sectional area (T.Ar) with a proportional decrease in marrow area (M.Ar), in male but not female mice, indicating inhibition of radial bone expansion (**Supplementary Figs. 2A-J**). Reduction in T.Ar in male mice was associated with reduced mean polar moment of inertia (**Supplementary Figs. 2 B, D**). In the trabecular bone compartment at the femur distal metaphysis, Val-R-fed female mice showed reduced trabecular thickness, suggesting reduced bone remodeling (**Supplementary Figs. 2G, H-J**).

While decreased weight and adiposity can result from reduced calorie intake, this was not the case; in fact, Val-R-fed mice consume more calories (but less valine) relative to their body weight than CTL-fed mice (**Figs. 2A-D**). We therefore examined energy balance in detail using metabolic chambers. In both males and females, Val-R significantly increased energy expenditure at 18 months of age (**Figs. 2E-F & 2H-I**); we observed a similar overall effect of diet on energy expenditure throughout the lifespan, reaching statistical significance at 12, 18, and in males, 24 months of age (**Figs. 2G, 2J**). Although the CTL and Val-R diets have an identical percentage of calories derived from amino acids, carbohydrates, and fats, there was an overall effect of diet on the respiratory exchange ratio (RER) in both sexes, with RER higher in Val-R-fed males than CTL-fed males throughout their life, and RER higher in Val-R-fed females prior to 24 months of age (**Supplementary Figs. 3A-B**). The increased energy expenditure of Val-R-fed mice was not the result of increased activity; spontaneous activity was not altered by a Val-R diet in males and was lower, not higher, in Val-R fed females than in CTL-fed females (**Supplementary Figs. 3C-D**).

The effects of PR on energy balance are mediated by the energy balance hormone fibroblast growth factor 21 (FGF21), in part by promoting the beiging of inguinal white adipose tissue (iWAT) [16,55-60]. However, we observed no increase in FGF21 in Val-R fed mice (**Figs. 2K**). We also observed no change in the phosphorylation of eIF2α in the liver or muscle

(**Supplementary Figs. 3E-K**), which is upstream of FGF21 [61-63], suggesting that an increase in FGF21 does not mediate the metabolic effects of Val-R. While we previously reported that Val-R induces beiging in young C57BL/6J mice [22], consistent with the lack of induction of FGF21 in the present study, the iWAT adipocytes of Val-R-fed mice at 24 months of age were monolocular and of similar size to that of CTL-fed mice (**Figs. 2L-M**). Despite this lack of change in the adipocyte morphology, there was an overall significant effect of diet on thermogenic gene expression, with a significant increase in the expression of *Elovl3,* but not *Ucp1* or *Cidea*, in Val-R-fed mice of both sexes (**Figs. 2N-O**), suggesting that Val-R may induce alterations in lipid metabolism rather than UCP1-dependent thermogenesis. We also observed decreased monolocular fat in the brown adipose tissue (BAT) of Val-R fed mice as compared to their CTL-fed counterparts, which was significantly different in males (**Supplementary Figs. 3M-N**), suggesting a shift away from lipid storage and towards utilization of lipids for thermogenesis. In support of this we observed increased expression of *Elovl3* in the BAT as well as increases in lipolysis- and lipogenesis-related genes in the BAT of both sexes (**Supplementary Figs. 3O-P**), suggesting an upregulation of futile cycling to promote thermogenesis. Overall, this data suggests that the increased energy expenditure of Val-R fed mice is mediated by increased BAT thermogenesis via a mechanism independent of the FGF21-UCP1 axis.

We examined the effect of Val-R on glycemic control longitudinally throughout life. Val-R-fed males displayed improved glucose tolerance as early as 3 months of age and throughout life, even at 24 months of age (**Figs. 3A-C, Supplementary Figs. 4A-B, E-F, I-J, M-N**). Val-R-fed males tended to be more sensitive to I.P. administration of insulin than CTL-fed males, which was significant at 12 months of age (**Figs. 3D-F**). While we observed no significant difference in glucose-stimulated insulin secretion (GSIS) nor HOMA2-IR (**Figs. 3G-H**), we did observe an improvement in HOMA2 %B, suggesting Val-R improved pancreatic beta cell function (**Fig. 3I**). Additionally, we tested for suppression of hepatic gluconeogenesis by performing an alanine tolerance test (ATT). We found a significant overall effect of diet, suggesting that Val-R improves hepatic insulin sensitivity in males (**Supplementary Fig. 4Q**).

Val-R-fed females similarly had improved glucose tolerance throughout the majority of their life (**Figs. 3J-L, Supplementary Figs. 4C-D, G-H, K-L, O-P**). In contrast to males, there was no overall effect of Val-R on the response to I.P. administration of insulin (**Figs. 3N-P**). As in males, the Val-R diet had no significant differences in GSIS nor HOMA2-IR in females, but increased beta cell function as measured via HOMA2 %B (**Fig. 3P-R**). Also as in males, a Val-R diet had an overall effect of diet on alanine tolerance suggestive of improved hepatic insulin sensitivity (**Supplementary Fig. 4R**). Overall, we found that Val-R-fed mice of both sexes had improved glycemic control relative to their CTL-fed counterparts.

Hepatic insulin sensitivity is strongly influenced by hepatic lipid deposition. At 24 months of age, we assessed fatty liver using oil-red-O staining. We found that there was an overall effect of diet on lipid droplet size in both sexes, with Val-R-fed males having significantly smaller hepatic lipid droplets than CTL-fed males (**Figs. 3S-T**). While the overall area of lipids droplets decreased in response to a Val-R diet (**Fig. 3V**), the total number of lipid droplets increased in both sexes (**Fig. 3U**).

Overall, we find that consumption of a Val-R diet results in an overall improvement in metabolic health. Val-R reduces fat mass and adiposity, likely through an increase in energy expenditure mediated by increased iWAT or BAT thermogenesis, improves glycemic control, and protects from hepatic steatosis.

Tissue- and sex-specific effects of valine restriction

To investigate the molecular impact of Val-R across tissues, we performed transcriptional profiling of brown adipose tissue (BAT), liver and muscle of CTL-fed and Val-R-fed mice of both sexes at 24 months of age. As anticipated, principal component analysis (PCA) showed that gene expression profiles grouped strongly by tissue type (**Fig. 4A**). We visualized the top 50 most variable genes across samples and found that, overall, the muscle and BAT had much more similar gene expression patterns than the liver, with the exception of *Ucp1* which was much more highly expressed in BAT than in liver or muscle (**Fig. 4B**).

The response to Val-R was highly influenced by sex and tissue. Liver had by far the greatest number of differentially expressed genes in response to Val-R, with over 1,500 genes differentially expressed in both sexes. There were over 1,200 genes differentially expressed in Val-R-fed female BAT, but only 226 were differentially expressed in Val-R-fed male BAT. Similarly, over 700 genes were differentially expressed in Val-R-fed female muscle, but only 14 genes were differentially expressed in Val-R-fed male muscle. In males, no genes were significantly differentially expressed in response to Val-R across all three tissues, while in females, only five genes were shared between liver, BAT and muscle (**Fig. 4C**).

When we investigated the pathways enriched for each of the tissues, and compared males and females, we found many pathways altered by Val-R in the liver, with fewer pathways altered in muscle and BAT, and a strong sex-specific response in all tissues (**Fig. 4D**). In liver, there was an upregulation of the “Valine, leucine, and isoleucine degradation” pathway in females in Val-R mice. We further examined this pathway at the gene level; interestingly, the genes in this pathway have almost completely opposite responses to Val-R in males and females, suggesting that Val-R induces sex-specific shifts in hepatic BCAA catabolism (**Fig. 4E**). The strongest changes, as well as the most sex-specific, occurred in liver, with more modest effects in muscle and BAT (**Fig. 4E**).

There was also an upregulation in female liver of several metabolic pathways such as “Fatty acid degradation,” “TCA cycle,” and the metabolism of several other amino acids including methionine, tryptophan, arginine, and “Glycine, serine, and threonine metabolism.” This last has been previously associated with calorie-restriction-induced changes in longevity [64]. Several immune system pathways and cancer signaling pathways, including “FoxO signaling” and “p53 signaling” were downregulated in the livers of female mice. Many fewer pathways were altered in response to Val-R in the male liver, and a number of these were shared with females. Upregulated liver pathways in both sexes included “Arachidonic acid metabolism,” “Parkinson’s disease,” and “Alzheimer’s disease.” Downregulated pathways in both sexes included “Autophagy” and “Lysosome.” Pathways specifically altered in male liver included upregulation of “Ribosome” and “Ribosome biogenesis in eukaryotes.”

In the muscle, only “Autophagy” was upregulated in females in response to Val-R, while a number of metabolic pathways including “Steroid biosynthesis” and “Insulin signaling pathway” were upregulated in the BAT (**Fig. 4D**). No significant pathway changes induced by Val-R were seen in the BAT or muscle of male mice, although as noted in **Fig. 4E**, we observed altered expression of various genes involved in BCAA degradation. Further, while we saw histological BAT changes (**Supplementary Figs. 3M-N**), there was no pathway enrichment related to thermogenesis in either sex (**Fig. 4D**). Interestingly, when we looked directly at thermogenic genes in our BAT transcriptomics, we found an upregulation of *Elovl3* as well as lipolytic and lipogenic genes in males and females (**Supplementary Figs. 3M-N**, p-values can be found in **Table S2**). We also looked at genes related to calcium futile cycling in the muscle and BAT and found largely no differences in muscle, but did find a female-specific increase in some genes (p-values can be found in **Table S2**), suggesting calcium futile cycling may play a sex-specific role in the increased thermogenesis in Val-R-fed mice. Further work will be necessary to understand the physiological and molecular mechanisms by which Val-R affects energy expenditure, as well as how this may vary by age.

A particularly surprising aspect of these results is that amino acids in general and the BCAAs in particular are agonists of mTORC1; we have previously shown that protein or BCAA restriction reduces mTORC1 signaling in the muscle and liver as well as other tissues [23,41,65,66]. While some of the pathways identified from transcriptional profiling were consistent with decreased mTORC1 – in particular, the upregulation of “Autophagy” in liver and muscle, and downregulation of “Lysosome” in the liver – others, including the male-specific increase in “Ribosome and Ribosome biogenesis”, suggested that hepatic mTORC1 signaling might actually increase in Val-R-fed males.

To clarify the effect of Val-R on mTORC1 and autophagy, we examined these in more detail at the protein level. In the muscle, there was no statistically significant effect of diet on mTORC1 signaling in males as assessed by the phosphorylation of the mTORC1 substrates S6K1 T389 and 4E-BP1 T37/S46, or the mTORC1 downstream readout S6 S240/S244 (**Supplementary Figs. 5A-B**). In females, we saw a trend (p=0.0594) towards reduced mTORC1 signaling in Val-R fed females and no difference in autophagy (**Supplementary Figs. 5D-E**). This surprisingly did not match with our transcriptomic finding, as the only significant KEGG pathway we found altered by Val-R in muscle was “Autophagy” in females.

In the liver, we found a significant effect of diet on mTORC1 signaling in both males and females, with a statistically significant increase in the phosphorylation of the mTORC1 substrate S6K1 T389 in both sexes (**Figs. 5A-B, D-E**). In the livers of males, but not females, we found an overall significant effect of Val-R on autophagy, with significant decreases in the level of LC3 and LC3 cleavage (p=0.0987) (**Figs. 5C and 5F**). These results generally agree with our transcriptional profiling of the liver, which suggested increased activity of mTORC1 in the liver.

A key hallmark of aging is cellular senescence [67,68]; mTORC1 signaling promotes senescence and SASP production [69-72]. We therefore hypothesized that the increased hepatic mTORC1 activity in Val-R-fed mice would result in an increase in senescence. Staining for the cellular senescence marker SA-β-Gal, we found that in response to Val-R, there was a significant diet effect. However, Val-R acted to reduce SA-βGal rather than to our hypothesized increase

(**Fig. 5G-H**), more in alignment with our recent finding that dietary restriction of BCAAs reduces hepatic senescence [30]. Looking in other tissues, we found a significant effect of diet in the kidney, with a strong diet-sex interaction consistent with a reduction of cellular senescence by Val-R in females but not males (**Supplementary Figs. 5G-H**). In the spleen, we found no overall effect of diet on cellular senescence (**Supplementary Figs. 5I-J**).

Valine restriction reduces neuroinflammation in both sexes and improves short-term memory in females

Restriction of dietary protein or BCAAs preserves cognition in the context of Alzheimer's disease [41,73]. To assess the effects of Val-R on cognitive function during normal aging, we performed a novel object recognition (NOR) test on the mice at 27 months of age. We found that there was a diet-sex interaction (p=0.0543) on short-term memory, with Val-R fed females, but not males, showing an improved ability to recognize the novel object compared to their CTL-fed counterparts (**Fig. 6A**). In contrast, neither sex displayed improvements in long-term memory with Val-R feeding (**Fig. 6B**).

Neuroinflammation commonly increases with age and is associated with cognitive decline as well as age-related diseases such as Alzheimer's disease [74-77]. We assessed neuroinflammation by looking at the activation of microglia and astrocytes through immunostaining brain sections with anti-glial fibrillary acidic protein (GFAP), an astrocyte marker, or anti-ionized calcium binding adaptor molecule 1 (IBA-1), a microglia marker. We looked at the arcuate nucleus (Arc) of the hypothalamus, a region critical for energy homeostasis as well as the sub-regions of the hippocampus, the CA3 region and the dentate gyrus (DG), which play a role in memory acquisition and memory retrieval. We found that Val-R reduces IBA1 in all three regions of the brain in male mice (**Figs. 6C-H**), and reduced GFAP in the Arc and CA3 of Val-R males (**Supplementary Figs. 6A-F**). Val-R also reduced IBA1 in the Arc of females, and significantly reduced GFAP in the DG of females (**Figs. 6C-D and Supplementary Figs. 6C-D**). However, this is most likely due to the significant overall effect of sex on IBA1 staining of CA3 and DG, and GFAP staining of all regions, due to the substantially lower levels of IBA and GFAP in females than males (**Figs. 6C-H and Supplementary Figs. 6A-F**). We also saw a significant diet x sex interaction in IBA1 staining of the Arc, which we interpret as the effect of Val-R being larger in males than in females (**Figs. 6C-H**).

Valine restriction improves healthspan and lifespan

We comprehensively assessed healthspan in mice as they age. Mice and humans become increasingly frail with age, and starting at approximately 12 months of age, we utilized a widely-adopted mouse frailty index [38] to assess the impact of Val-R on frailty in both sexes. We observed that in both males and females, Val-R feeding resulted in a lower frailty index as compared to their CTL-fed counterparts over time (**Figs. 7A-B**). The reduced frailty in Val-R fed mice was primarily the result of decreased deficits in the "Physical/Musculoskeletal" and "Discomfort" categories (**Supplementary Figs. 7A-L**).

We also performed rotarod and inverted cling assays to assess muscle coordination and grip strength, respectively. In both males and females, we found no difference in muscle coordination with Val-R feeding as measured by rotarod performance (**Figs. 7C, E, Supplementary Figs. 8A-C, E-F**), while time did seem to reduce performance regardless of diet. In Val-R-fed males, we observed a significant overall improvement in grip strength as measured by an inverted cling assay, which reached statistical significance at every age measured (**Fig. 7D**). Analyzing performance on these assays using weight as a covariate, however, suggests the effects of Val-R on inverted cling performance are primarily the effect of lower weight (**Supplementary Figs. 8A-F**). In Val-R-fed females, we saw a significant overall impact of diet on inverted cling performance that did not reach significance at any single age (**Fig. 7F**). When analyzed by ANVOCA, Val-R-fed females performed worse on the rotarod than CTL-fed females at all time points, reaching statistical significance at 12 and 24 months of age, and Val-R-fed females had slightly worse, though not significantly so, inverted cling performance than CTL-fed females at all ages (**Supplementary Figs. 8G-L**). Additionally, when using ANCOVA to test for body weight as a covariate for inverted cling performance, we found that this test could not be performed at 24 months of age in males because their slopes reached statistical significance, and therefore, could not be compared (**Supplementary Figs. 8E-F**). To address the issue of comparing the groups using ANCOVA, we attempted to normalize the effect of body weight by multiplying the inverted cling time by the weight of each mouse to determine the amount of work the animals are doing. We found that in males and not females, Val-R had increased time x grams of body weight at every timepoint, suggesting that they may be doing more work (**Supplementary Figs. 8M-N**). Overall, these results are consistent with Val-R having minimal effects on muscles except perhaps promoting strength in aged mice.

Lower urinary tract dysfunction increases with age [78,79]. We assessed urinary frequency, and we found that Val-R-fed males had significantly less urinary spotting compared to their CTL-fed counterparts (**Fig. 7G**); no difference was observed in females (**Fig. 7G**).

Cancer is a major cause of death in C57BL6/J mice [80-82]. Upon natural death or meeting criteria for euthanasia, we performed a gross necropsy in mice followed to the end of their life. We found that Val-R reduced the prevalence of cancer observed at necropsy in both male (p=0.0559) and female (p=0.0275) mice (**Fig. 7H**).

Lastly, in agreement with the reduction in frailty, improved health metrics and reduced cancer incidence, we found that the lifelong consumption of a Val-R diet extends lifespan (p=0.03, log-rank test stratified by diet) (**Fig. 7I**). Cox regression likewise indicated a significant effect of diet on survival (hazard rate (HR) = 0.0163), and no interaction of genotype with sex was detected (**Fig. 7I**). Further, when assessing sexes separately, we found a 23.42% increase in the median lifespan and a significant extension of the maximum lifespan of male Val-R-fed mice (Wang-Allison, p=0.02575), but not female lifespan (**Fig. 7I-L**). Investigating the survival of the top 10 longest-lived animals in each group, we found the top 10 Val-R males had a 14.15% increase in lifespan relative to the top 10 of CTL-fed males; the top 10 Val-R-fed females displayed a 7.07% increase in maximum lifespan compared to the top 10 CTL-fed females (**Fig. 7M**).

Lastly, using the cumulative data on longevity, frailty, healthspan and hallmarks of aging collected during this lifespan study, we assessed FAMY (Frailty Adjusted Mouse Years) and

GRAIL (Gauging Robust Aging when Increasing Lifespan), new summary statistics that are analogous to Quality Adjusted Life Years (QALY) in humans [54]. In response to Val-R, we see increases in FAMY and GRAIL in males, with a 20.29% increase in FAMY and a 33.05% increase in GRAIL (**Fig**. **7N-O**). In females, while we do see an 11.89% increase in FAMY, it is not statistically significant; however, GRAIL increases by 28.84% (**Fig**. **7N-O**). Overall, these data demonstrate that Val-R increases healthspan in both males and females.

In summary, we find that lifelong Val-R results in both general and sex-specific improvements in both health and lifespan. Val-R reduces body weight and adiposity, which may be mediated by an increase in energy expenditure, as well as promoting blood sugar control across the lifespan. We see that Val-R reduces hepatic steatosis in both sexes, but particularly in males. Surprisingly, despite reduced dietary levels of valine, Val-R-fed mice have increased hepatic mTOR signaling; yet a Val-R diet reduced hepatic senescence. We found that Val-R improves cognition in female STM while reducing neuroinflammation in both sexes, reduces frailty and cancer prevalence in both sexes, and improves urinary function in males. Val-R extends median lifespan by 23% and maximum lifespan by 14.15% in males, while extending maximum lifespan in females by 7.07%. We also confirmed an overall improvement in healthspan in response to Val-R in both sexes through the assessment of FAMY and GRAIL.

To gain more mechanistic insight into the effects of Val-R, we performed a weighted gene co-expression network analysis (WGCNA). Selected traits and pathways for males and females are shown in **Fig. 8** and **Supplementary Fig. 9**; full tables and pathways can be found in **Tables S9-S12**. In males, we observed that the turquoise module had several strongly correlated phenotypes, including body composition, valine intake, hepatic lipid droplet size and brain inflammation traits (**Fig. 8A**). Pathway enrichment on the genes in the turquoise module showed that the genes in this module were enriched for changes in processes related metabolism and longevity pathways, such as the “PI3K-Akt pathway”, “MAPK signaling”, “AGE-RAGE signaling pathway in diabetic complications” and “metabolic pathways” (**Figs. 8B**). We looked into the significantly altered genes within the PI3K-Akt and MAPK signaling pathways, and we found that only the PI3K-Akt pathway, and not the MAPK signaling pathway, was downregulated in males (**Figs. 8C-D, Supplementary Fig. 9C**), suggesting a potential role in the downregulation of PI3K-Akt signaling in the lifespan extension in males.

In females, we observed that the blue module had a strong negative correlation with autophagy and a positive correlation with lean mass (**Supplementary Fig. 9A**). When we performed pathway enrichment on the genes clustered into the blue module, we found only 3 pathways that had changes in all three tissues (“hematopoietic cell lineage”, “intestinal immune network for IgA production” and “cytokine-cytokine receptor interaction”) that do not have known associations with aging (**Supplementary Fig. 9B**).

Discussion

Dietary macronutrient composition is a major regulator of healthy aging, with dietary protein emerging as a key regulator of longevity and health in both humans and rodents [6,11,12,15-17,26,43]. Restriction of protein, BCAAs and isoleucine alone are sufficient to promote healthy aging and extend lifespan in mice [22,24-26,65]. However, the roles of leucine and valine remain in healthy

aging have not yet been closely examined. Here, we focused on valine, motivated by emerging data linking it to adverse metabolic effects as well as cancer and inflammation [22,31-35,83]. We hypothesized that valine restriction (Val-R) would improve healthspan and extend longevity. We found that lifelong Val-R improved weight, adiposity, glycemic control, and energy balance in both sexes, extended lifespan in males, and reduced frailty in both males and females.

Val-R has both similarities and differences from other amino acid restrictive diets. Like isoleucine restriction and methionine restriction, Val-R extends male lifespan, but unlike the others, fails to extend female lifespan [19,20,24,26,84-89]. All three interventions improve glucose tolerance, reduce frailty, protect against liver pathology and cancer, and increase energy expenditure, partly through white adipose tissue thermogenesis [20,22,26,90,91]. Val-R uniquely fails to improve rotarod performance [20,26], and induces distinct effects on cognition and neuroinflammation that have not been fully characterized in other dietary interventions.

At the molecular level, Val-R is distinct from isoleucine and methionine restriction. While isoleucine, methionine and short-term Val-R all induce circulating FGF21, long-term Val-R does not [22,26,30,90,91]. Unlike methionine restriction, which suppresses mTORC1, Val-R increases hepatic mTORC1 activity while leaving mTORC1 in the muscle unchanged [90,92]. Moreover, Val-R decreases hepatic autophagy, an unexpected finding given the positive links between autophagy and longevity [93-96]. Differences in amino acid catabolism may underlie some of these effects: methionine catabolism yields the methyl donor SAM, while isoleucine catabolism generates both acetyl-CoA and succinyl-CoA, whereas valine catabolism yields only succinyl-CoA.

Val-R showed strong sex-specific responses. Nearly every gene in the BCAA degradation pathway changed in the opposite direction in males and females. Specifically, *Bckdha* and *Bckdhb*, genes which encode the rate limiting enzyme of BCAA degradation step in the liver, were downregulated in males only. One possible explanation for this difference is that males may be more valine restricted, while perhaps females retain greater BCAA availability, possibly explaining the extension of male but not female lifespan. Differences in BCAA catabolism between the sexes has been observed in previous studies [26,97-99]. Our transcriptional analysis found that “Valine, leucine, and isoleucine degradation” – as well as pathways related to the metabolism or biosynthesis of many other amino acids, including alanine, arginine, aspartate, cysteine, glutamate, methionine, proline, tryptophan, and tyrosine – were significantly upregulated in the livers of Val-R-fed females, but not in Val-R-fed males. Although frailty is closely correlated with longevity in both mice and humans [100-102], Val-R reduced frailty in females without extending their lifespan. We previously observed this uncoupling in protein restricted UM-HET3 females [26,54]. Perhaps 67% restriction of dietary valine is sufficient to improve multiple health metrics in female mice, but is insufficient to extend female lifespan; if so, future studies could explore if a greater degree of restriction could also extend female lifespan.

When we specifically investigated the genes related to BCAA degradation, we found that the strongest changes in these genes were in the liver, with smaller changes in muscle and BAT. Further, there was a strong effect of sex on the response of hepatic BCAA degradation genes to Val-R, with females primarily upregulating BCAA degradation genes in response to Val-R and males downregulating the same genes. There were only 7 genes in which males and females responded in a similar manner in the liver. Notably, *Hmcgl, Aldh3a2* and *Acat1* were

downregulated in both sexes, while *Acaa2* and *Acadm* were upregulated in both sexes; all of these genes play a role in lipid and fatty acid metabolism. This supports others' findings that valine alters fatty acid metabolism to impact fatty liver disease [34,103-105]. Further, we see a diet effect in reducing lipid droplet size and count in our male and female Val-R-fed mice. While there were some differences in the response of male and female BCAA degradation genes in muscle, there was a minimal effect of sex on the response to Val-R in BAT. Overall, these results were unexpected, as muscle is the primary site of BCAA catabolism, and is traditionally thought of as very sexually dimorphic; and at the molecular level, liver, muscle and adipose have similar levels of sexually dimorphic gene expression [106]. Understanding sex-specific differences in BCAA and AA metabolism may be important to understanding the basis for the beneficial and sex-specific impacts of Val-R and other diets on healthy aging.

Val-R also protects from hepatic senescence, a cell-cycle arrested state. It was recently shown that mTOR activity oscillates through the cell cycle, with high activity during the growth-related S and G2 phases to promote progression through these phases and lower activity during the mitosis and G1 phases to induce an autophagic response [107]. Perhaps, the increased mTORC1 and reduced autophagy we see in our Val-R animals may be due to them progressing through the cell cycle rather than being stalled in an arrested state. We have also shown that BCAA restriction protects from hepatic mitochondrial dysfunction [30] so perhaps, Val-R may mediate health and lifespan similarly.

Despite weight-normalized preservation of muscle mass, Val-R did not consistently improve functional performance. Inverted cling tests suggested modest benefits, but these were largely attributable to reduced body weight. We also saw benefits of Val-R on frailty, particularly with the physical/musculoskeletal scoring. We did not measure muscle strength, quality, or fiber type, which will be critical to examine in future studies examining how valine impacts muscle.

WGCNA analysis implicated PI3K-Akt, AGE-RAGE and MAPK signaling across liver, muscle and adipose tissue, with changes in males consistent with improved health and longevity [108-117]. Cellular senescence and related pathways (i.e. p53 signaling and NF Kappa B signaling) as well as type 2 diabetes and insulin secretion were also altered, particularly in the liver, further supporting the role of valine on health; and these findings are supported by our recent finding that BCAA restriction inhibits hepatic senescence [118]. In females, we found an overall weaker correlation of modules to phenotypic traits, and in the blue module where the strongest associations were found, we observed only a partial enrichment for PI3K-Akt and MAPK signaling. There was no observable pattern in significant genes altered in the PI3K-Akt signaling pathway in Val-R-fed females; this further supports the downregulation of PI3K-Akt signaling found in Val-R-fed males mediates their lifespan extension.

When we looked specifically at the genes altered in the PI3K-Akt pathway in Val-R-fed males, we found that *Spp1*, which encodes osteopontin, a multifunctional protein involved in bone metabolism, inflammation, and cancer, was decreased in all three tissues. SPP1 is increased in chronic liver disease and hepatocellular carcinoma and is associated with poor prognosis in humans [119,120], and loss of osteopontin protects from senescent phenotypes in aging adipose tissue and promote adipogenesis [121,122]. *Spp1+* macrophages have also been shown to accumulate in aging skeletal muscle and in multiple forms of cancer as well as promote

intracellular fat accumulation in dystrophic muscle [123-128]. Future studies should assess the role of the PI3K-Akt pathway generally and *Spp1* specifically in the lifespan and healthspan benefits of Val-R mice.

There are several limitations of the work we conducted here. First, we examined only a single level of restriction. Studies of CR, PR, and geroprotective drugs like rapamycin have shown that different levels of restriction or drugs can yield different responses [15,129-132]. Different levels of Val-R may be able to extend female lifespan and healthspan, and examining the graded response to Val-R may provide new insights into biological mechanisms as well as the basis for the sex-specific effects we observed. We analyzed longevity in only a single inbred strain of mice, C57BL/6J, and commenced our study when the mice were only 4 weeks old. There were advantages to this approach – in particular, the strain and age of onset were chosen to match conditions under which PR and BCAA restriction were previously shown to extend male lifespan by over 30% [17]. However, different strains of mice can have different responses to lifespan interventions [130,133], and interventions that begin later in life are more likely to be translatable than interventions begun in extremely young animals. Future studies of Val-R should be conducted in other strains of mice – for instance, genetically heterogeneous UM-HET3 mice which better mimic the genetic variability found in the human population – and begin Val-R in fully adult mice.

The diets we used here are extremely well-controlled, and are isocaloric, matched for the quantity and source of carbohydrates and fats, and isonitrogenous. However, choices still had to be made; the diets used here are based on the AA profile of a whey-based diet; and the reduction of valine was balanced by a small increase in a number of non-essential AAs. The protein-to-carbohydrate ratio, the type and levels of dietary carbohydrates and fats consumed, or the ratio of different amino acids to valine could all play a role in the responses we observed. The optimal level of protein may vary by age – it is generally believed that older people need to consume more protein – and varying levels of valine at different ages could lead to different results.

In conclusion, we have shown that dietary restriction of valine can promote healthy aging in both sexes, and extend the lifespan of male, but not female mice. Our results are consistent with a growing consensus showing that higher levels of valine are associated with negative impacts on healthy aging, including insulin resistance, cardiovascular disease, and cancer. Additional research will be required to identify the optimal level of dietary valine, especially across mice of different sexes, ages, and genetic background, and to identify if there are negative consequences to valine restriction. Our results highlight how protein quality, the specific amino acids that make up the protein, is as important in mediating healthy aging as total protein or the number of calories. While additional tests need to done to fully understand how valine affects health in humans, our results support the idea that lowering the amount of dietary valine may promote healthy aging.

Conflict of Interests

D.W.L. has received funding from, and is a scientific advisory board member of, Aeovian Pharmaceuticals, which seeks to develop novel, selective mTOR inhibitors for the treatment of various diseases.

Author Contributions

Experiments were performed in the Lamming laboratory, except for the analysis of the brain IHC, which was performed in the Sadagurski lab and the microCT analysis on the femur bone, which was performed in the Yakar lab. MC, MS, SY, WAR and DWL conceived the experiments and secured funding. MFC, IA, PL, SML, LEB, HSMJ, DNHM, SY, TL, CLG, RB, MMS, YL, IG, CYY, YL, and BK performed the experiments. MC, HSMJ, CLG, TL, MS and DWL analyzed the data. MFC, CLG, MS, and DWL wrote the manuscript.

Funding

The Lamming lab is supported in part by the NIA (AG056771, AG081482, AG084156, AG085898, AG094153), the NIDDK (DK125859), and startup funds from UW-Madison. MFC is supported by F31AG082504. CLG was supported in part by Dalio Philanthropies, a Glenn Foundation Postdoctoral Fellowship, and by Hevolution Foundation award HF-AGE AGE-009. RB was supported by F31AG081115. C-Y.Y. was supported in part by a NIA F32 postdoctoral fellowship (F32AG077916) and a NIA K99 award (K99AG084921). The Sadagurski lab is supported in part by the NIEHS (R01ES033171) and NIA (RF1AG078170). T.T.L. was supported by K01 AG059899. The authors used the UW-Madison Biotechnology Center Gene Expression Center (RRID:SCR_017757) which is supported in part by the UW Carbone Cancer Center (UWCCC) (P30CA014520). The UWCCC Experimental Animal Pathology Laboratory is supported by P30 CA014520 from the NIH/NCI. W.A.R and D.W.L. are members of the Wisconsin Nathan Shock Center of Excellence in the Basic Biology of Aging, P30 AG092586. The Lamming lab was supported in part by the U.S. Department of Veterans Affairs (I01-BX004031 and IS1-BX005524), and this work was supported using facilities and resources from the William S. Middleton Memorial Veterans Hospital. The content is solely the responsibility of the authors and does not necessarily represent the official views of the NIH. This work does not represent the views of the Department of Veterans Affairs or the United States Government.

References

1. Green, C.L., Lamming, D.W., and Fontana, L. (2022). Molecular mechanisms of dietary restriction promoting health and longevity. Nat Rev Mol Cell Biol *23*, 56-73. 10.1038/s41580-021-00411-4.
2. Mihaylova, M.M., Chaix, A., Delibegovic, M., Ramsey, J.J., Bass, J., Melkani, G., Singh, R., Chen, Z., Ja, W.W., Shirasu-Hiza, M., et al. (2023). When a calorie is not just a calorie: Diet quality and timing as mediators of metabolism and healthy aging. Cell Metab *35*, 1114-1131. 10.1016/j.cmet.2023.06.008.
3. Moon, J., and Koh, G. (2020). Clinical Evidence and Mechanisms of High-Protein Diet-Induced Weight Loss. J Obes Metab Syndr *29*, 166-173. 10.7570/jomes20028.
4. Paddon-Jones, D., Westman, E., Mattes, R.D., Wolfe, R.R., Astrup, A., and Westerterp-Plantenga, M. (2008). Protein, weight management, and satiety. Am J Clin Nutr *87*, 1558S-1561S. 10.1093/ajcn/87.5.1558S.
5. Coelho-Junior, H.J., Rodrigues, B., Uchida, M., and Marzetti, E. (2018). Low Protein Intake Is Associated with Frailty in Older Adults: A Systematic Review and Meta-Analysis of Observational Studies. Nutrients *10*. 10.3390/nu10091334.
6. Levine, M.E., Suarez, J.A., Brandhorst, S., Balasubramanian, P., Cheng, C.W., Madia, F., Fontana, L., Mirisola, M.G., Guevara-Aguirre, J., Wan, J., et al. (2014). Low protein intake is

associated with a major reduction in IGF-1, cancer, and overall mortality in the 65 and younger but not older population. Cell Metab *19*, 407-417. 10.1016/j.cmet.2014.02.006.

7. Sluijs, I., Beulens, J.W.J., van der A, D.L., Spijkerman, A.M.W., Grobbee, D.E., and van der Schouw, Y.T. (2009). Dietary Intake of Total, Animal, and Vegetable Protein and Risk of Type 2 Diabetes in the European Prospective Investigation into Cancer and Nutrition (EPIC)-NL Study. Diabetes Care *33*, 43-48. 10.2337/dc09-1321.
8. van Nielen, M., Feskens, E.J.M., Mensink, M., Sluijs, I., Molina, E., Amiano, P., Ardanaz, E., Balkau, B., Beulens, J.W.J., Boeing, H., et al. (2014). Dietary Protein Intake and Incidence of Type 2 Diabetes in Europe: The EPIC-InterAct Case-Cohort Study. Diabetes Care *37*, 1854-1862. 10.2337/dc13-2627.
9. Lagiou, P., Sandin, S., Weiderpass, E., Lagiou, A., Mucci, L., Trichopoulos, D., and Adami, H.O. (2007). Low carbohydrate-high protein diet and mortality in a cohort of Swedish women. J Intern Med *261*, 366-374. 10.1111/j.1365-2796.2007.01774.x.
10. Ni Lochlainn, M., Bowyer, R.C.E., Welch, A.A., Whelan, K., and Steves, C.J. (2023). Higher dietary protein intake is associated with sarcopenia in older British twins. Age Ageing *52*. 10.1093/ageing/afad018.
11. Ferraz-Bannitz, R., Beraldo, R.A., Peluso, A.A., Dall, M., Babaei, P., Foglietti, R.C., Martins, L.M., Gomes, P.M., Marchini, J.S., Suen, V.M.M., et al. (2022). Dietary Protein Restriction Improves Metabolic Dysfunction in Patients with Metabolic Syndrome in a Randomized, Controlled Trial. Nutrients *14*. 10.3390/nu14132670.
12. Fontana, L., Cummings, N.E., Arriola Apelo, S.I., Neuman, J.C., Kasza, I., Schmidt, B.A., Cava, E., Spelta, F., Tosti, V., Syed, F.A., et al. (2016). Decreased Consumption of Branched-Chain Amino Acids Improves Metabolic Health. Cell reports *16*, 520-530. 10.1016/j.celrep.2016.05.092.
13. Nicolaisen, T.S., Lyster, A.E., Sjoberg, K.A., Haas, D.T., Voldstedlund, C.T., Lundsgaard, A.M., Jensen, J.K., Madsen, E.M., Nielsen, C.K., Bloch-Ibenfeldt, M., et al. (2025). Dietary protein restriction elevates FGF21 levels and energy requirements to maintain body weight in lean men. Nat Metab *7*, 602-616. 10.1038/s42255-025-01236-7.
14. Babygirija, R., Sonsalla, M.M., Han, J.H., James, I., Green, C.L., Calubag, M.F., Mill, J., Wade, G., Tobon, A., Michael, J., et al. (2023). Protein restriction slows the development and progression of Alzheimer's disease in mice. Res Sq. 10.21203/rs.3.rs-3342413/v1.
15. Green, C.L., Pak, H.H., Richardson, N.E., Flores, V., Yu, D., Tomasiewicz, J.L., Dumas, S.N., Kredell, K., Fan, J.W., Kirsh, C., et al. (2022). Sex and genetic background define the metabolic, physiologic, and molecular response to protein restriction. Cell Metab *34*, 209-226 e205. 10.1016/j.cmet.2021.12.018.
16. Hill, C.M., Albarado, D.C., Coco, L.G., Spann, R.A., Khan, M.S., Qualls-Creekmore, E., Burk, D.H., Burke, S.J., Collier, J.J., Yu, S., et al. (2022). FGF21 is required for protein restriction to extend lifespan and improve metabolic health in male mice. Nature communications *13*, 1897. 10.1038/s41467-022-29499-8.
17. Richardson, N.E., Konon, E.N., Schuster, H.S., Mitchell, A.T., Boyle, C., Rodgers, A.C., Finke, M., Haider, L.R., Yu, D., Flores, V., et al. (2021). Lifelong restriction of dietary branched-chain amino acids has sex-specific benefits for frailty and lifespan in mice. Nat Aging *1*, 73-86. 10.1038/s43587-020-00006-2.
18. Mair, W., Piper, M.D., and Partridge, L. (2005). Calories do not explain extension of life span by dietary restriction in Drosophila. PLoS Biol *3*, e223. 10.1371/journal.pbio.0030223.
19. Orentreich, N., Matias, J.R., DeFelice, A., and Zimmerman, J.A. (1993). Low methionine ingestion by rats extends life span. The Journal of nutrition *123*, 269-274. 10.1093/jn/123.2.269.

20. Miller, R.A., Buehner, G., Chang, Y., Harper, J.M., Sigler, R., and Smith-Wheelock, M. (2005). Methionine-deficient diet extends mouse lifespan, slows immune and lens aging, alters glucose, T4, IGF-I and insulin levels, and increases hepatocyte MIF levels and stress resistance. Aging Cell *4*, 119-125. 10.1111/j.1474-9726.2005.00152.x.
21. Yap, Y.W., Rusu, P.M., Chan, A.Y., Fam, B.C., Jungmann, A., Solon-Biet, S.M., Barlow, C.K., Creek, D.J., Huang, C., Schittenhelm, R.B., et al. (2020). Restriction of essential amino acids dictates the systemic metabolic response to dietary protein dilution. Nature communications *11*, 2894. 10.1038/s41467-020-16568-z.
22. Yu, D., Richardson, N.E., Green, C.L., Spicer, A.B., Murphy, M.E., Flores, V., Jang, C., Kasza, I., Nikodemova, M., Wakai, M.H., et al. (2021). The adverse metabolic effects of branched-chain amino acids are mediated by isoleucine and valine. Cell Metab *33*, 905-922 e906. 10.1016/j.cmet.2021.03.025.
23. Yeh, C.Y., Chini, L.C.S., Davidson, J.W., Garcia, G.G., Gallagher, M.S., Freichels, I.T., Calubag, M.F., Rodgers, A.C., Green, C.L., Babygirija, R., et al. (2024). Late-life protein or isoleucine restriction impacts physiological and molecular signatures of aging. Nat Aging *4*, 1760-1771. 10.1038/s43587-024-00744-7.
24. Fulton, T.L., Wansbrough, M.R., Mirth, C.K., and Piper, M.D.W. (2024). Short-term fasting of a single amino acid extends lifespan. Geroscience *46*, 3607-3615. 10.1007/s11357-024-01078-3.
25. Weaver, K.J., Holt, R.A., Henry, E., Lyu, Y., and Pletcher, S.D. (2023). Effects of hunger on neuronal histone modifications slow aging in Drosophila. Science *380*, 625-632. 10.1126/science.ade1662.
26. Green, C.L., Trautman, M.E., Chaiyakul, K., Jain, R., Alam, Y.H., Babygirija, R., Pak, H.H., Sonsalla, M.M., Calubag, M.F., Yeh, C.Y., et al. (2023). Dietary restriction of isoleucine increases healthspan and lifespan of genetically heterogeneous mice. Cell Metab *35*, 1976-1995 e1976. 10.1016/j.cmet.2023.10.005.
27. Mannick, J.B., and Lamming, D.W. (2023). Targeting the biology of aging with mTOR inhibitors. Nat Aging *3*, 642-660. 10.1038/s43587-023-00416-y.
28. Simcox, J., and Lamming, D.W. (2022). The central moTOR of metabolism. Dev Cell *57*, 691-706. 10.1016/j.devcel.2022.02.024.
29. Strong, R., Miller, R.A., Cheng, C.J., Nelson, J.F., Gelfond, J., Allani, S.K., Diaz, V., Dorigatti, A.O., Dorigatti, J., Fernandez, E., et al. (2022). Lifespan benefits for the combination of rapamycin plus acarbose and for captopril in genetically heterogeneous mice. Aging Cell *21*, e13724. 10.1111/acel.13724.
30. Calubag, M.F., Ademi, I., Grunow, I., Breuer, L., Babygirija, R., Lialios, P., Le, S., Minton, D., Sonsalla, M.M., Illiano, J., et al. (2025). Tissue-specific effects of dietary protein on cellular senescence are mediated by branched-chain amino acids. bioRxiv, 2025.2001.2013.632607. 10.1101/2025.01.13.632607.
31. Bidgood, C.L., Philp, L.K., Rockstroh, A., Lehman, M., Nelson, C.C., Sadowski, M.C., and Gunter, J.H. (2024). Targeting valine catabolism to inhibit metabolic reprogramming in prostate cancer. Cell Death & Disease *15*, 513. 10.1038/s41419-024-06893-2.
32. Bishop, C.A., Machate, T., Henning, T., Henkel, J., Puschel, G., Weber, D., Grune, T., Klaus, S., and Weitkunat, K. (2022). Detrimental effects of branched-chain amino acids in glucose tolerance can be attributed to valine induced glucotoxicity in skeletal muscle. Nutr Diabetes *12*, 20. 10.1038/s41387-022-00200-8.
33. Che, L., Liu, L., Xu, M., Fan, Z., Niu, L., Chen, Y., Chang, X., Zhou, P., Li, M., Deng, H., and Chen, W. (2024). Valine metabolite, 3-hydroxyisobutyrate, promotes lipid metabolism and

cell proliferation in porcine mammary gland epithelial cells. Front Nutr *11*, 1524738. 10.3389/fnut.2024.1524738.
34. Jang, C., Oh, S.F., Wada, S., Rowe, G.C., Liu, L., Chan, M.C., Rhee, J., Hoshino, A., Kim, B., Ibrahim, A., et al. (2016). A branched-chain amino acid metabolite drives vascular fatty acid transport and causes insulin resistance. Nat Med *22*, 421-426. 10.1038/nm.4057.
35. Zheng, H.Y., Wang, L., Zhang, R., Ding, R., Yang, C.X., and Du, Z.Q. (2024). Valine induces inflammation and enhanced adipogenesis in lean mice by multi-omics analysis. Front Nutr *11*, 1379390. 10.3389/fnut.2024.1379390.
36. Yu, D., Tomasiewicz, J.L., Yang, S.E., Miller, B.R., Wakai, M.H., Sherman, D.S., Cummings, N.E., Baar, E.L., Brinkman, J.A., Syed, F.A., and Lamming, D.W. (2019). Calorie-Restriction-Induced Insulin Sensitivity Is Mediated by Adipose mTORC2 and Not Required for Lifespan Extension. Cell reports *29*, 236-248 e233. 10.1016/j.celrep.2019.08.084.
37. Bellantuono, I., de Cabo, R., Ehninger, D., Di Germanio, C., Lawrie, A., Miller, J., Mitchell, S.J., Navas-Enamorado, I., Potter, P.K., Tchkonia, T., et al. (2020). A toolbox for the longitudinal assessment of healthspan in aging mice. Nature protocols *15*, 540-574. 10.1038/s41596-019-0256-1.
38. Whitehead, J.C., Hildebrand, B.A., Sun, M., Rockwood, M.R., Rose, R.A., Rockwood, K., and Howlett, S.E. (2014). A clinical frailty index in aging mice: comparisons with frailty index data in humans. J Gerontol A Biol Sci Med Sci *69*, 621-632. 10.1093/gerona/glt136.
39. Searle, S.D., Mitnitski, A., Gahbauer, E.A., Gill, T.M., and Rockwood, K. (2008). A standard procedure for creating a frailty index. BMC Geriatr *8*, 24. 10.1186/1471-2318-8-24.
40. Keil, K.P., Abler, L.L., Altmann, H.M., Bushman, W., Marker, P.C., Li, L., Ricke, W.A., Bjorling, D.E., and Vezina, C.M. (2016). Influence of animal husbandry practices on void spot assay outcomes in C57BL/6J male mice. Neurourol Urodyn *35*, 192-198. 10.1002/nau.22692.
41. Babygirija, R., Sonsalla, M.M., Mill, J., James, I., Han, J.H., Green, C.L., Calubag, M.F., Wade, G., Tobon, A., Michael, J., et al. (2024). Protein restriction slows the development and progression of pathology in a mouse model of Alzheimer's disease. Nature communications *15*, 5217. 10.1038/s41467-024-49589-z.
42. Calubag, M.F., Ademi, I., Yeh, C.Y., Babygirija, R., Pak, H.H., Bhoopat, A.M., Kasza, I., Green, C.L., Sonsalla, M.M., and Lamming, D.W. (2022). FGF21 has a sex-specific role in calorie-restriction-induced beiging of white adipose tissue in mice. Aging Biol *1*.
43. Cummings, N.E., Williams, E.M., Kasza, I., Konon, E.N., Schaid, M.D., Schmidt, B.A., Poudel, C., Sherman, D.S., Yu, D., Arriola Apelo, S.I., et al. (2018). Restoration of metabolic health by decreased consumption of branched-chain amino acids. The Journal of physiology *596*, 623-645. 10.1113/JP275075.
44. Jayarathne, H.S.M., Debarba, L.K., Jaboro, J.J., Ginsburg, B.C., Miller, R.A., and Sadagurski, M. (2022). Neuroprotective effects of Canagliflozin: Lessons from aged genetically diverse UM-HET3 mice. Aging Cell *21*, e13653. 10.1111/acel.13653.
45. Bouxsein, M.L., Boyd, S.K., Christiansen, B.A., Guldberg, R.E., Jepsen, K.J., and Muller, R. (2010). Guidelines for assessment of bone microstructure in rodents using micro-computed tomography. J Bone Miner Res *25*, 1468-1486. 10.1002/jbmr.141.
46. Pak, H.H., Haws, S.A., Green, C.L., Koller, M., Lavarias, M.T., Richardson, N.E., Yang, S.E., Dumas, S.N., Sonsalla, M., Bray, L., et al. (2021). Fasting drives the metabolic, molecular and geroprotective effects of a calorie-restricted diet in mice. Nat Metab *3*, 1327-1341. 10.1038/s42255-021-00466-9.
47. Lee, B.Y., Han, J.A., Im, J.S., Morrone, A., Johung, K., Goodwin, E.C., Kleijer, W.J., DiMaio, D., and Hwang, E.S. (2006). Senescence-associated beta-galactosidase is lysosomal beta-galactosidase. Aging Cell *5*, 187-195. 10.1111/j.1474-9726.2006.00199.x.

48. Dimri, G.P., Lee, X., Basile, G., Acosta, M., Scott, G., Roskelley, C., Medrano, E.E., Linskens, M., Rubelj, I., Pereira-Smith, O., and et al. (1995). A biomarker that identifies senescent human cells in culture and in aging skin in vivo. Proc Natl Acad Sci U S A *92*, 9363-9367. 10.1073/pnas.92.20.9363.
49. Zhao, J., Fuhrmann-Stroissnigg, H., Gurkar, A.U., Flores, R.R., Dorronsoro, A., Stolz, D.B., St Croix, C.M., Niedernhofer, L.J., and Robbins, P.D. (2017). Quantitative Analysis of Cellular Senescence in Culture and In Vivo. Curr Protoc Cytom *79*, 9 51 51-59 51 25. 10.1002/cpcy.16.
50. Melk, A., Schmidt, B.M., Takeuchi, O., Sawitzki, B., Rayner, D.C., and Halloran, P.F. (2004). Expression of p16INK4a and other cell cycle regulator and senescence associated genes in aging human kidney. Kidney Int *65*, 510-520. 10.1111/j.1523-1755.2004.00438.x.
51. Jiang, H., Lei, R., Ding, S.-W., and Zhu, S. (2014). Skewer: a fast and accurate adapter trimmer for next-generation sequencing paired-end reads. BMC Bioinformatics *15*, 182. 10.1186/1471-2105-15-182.
52. Dobin, A., Davis, C.A., Schlesinger, F., Drenkow, J., Zaleski, C., Jha, S., Batut, P., Chaisson, M., and Gingeras, T.R. (2013). STAR: ultrafast universal RNA-seq aligner. Bioinformatics *29*, 15-21. 10.1093/bioinformatics/bts635.
53. Li, B., and Dewey, C.N. (2011). RSEM: accurate transcript quantification from RNA-Seq data with or without a reference genome. BMC Bioinformatics *12*, 323. 10.1186/1471-2105-12-323.
54. Lamming, D.W. (2024). Quantification of healthspan in aging mice: introducing FAMY and GRAIL. Geroscience *46*, 4203-4215. 10.1007/s11357-024-01200-5.
55. Laeger, T., Henagan, T.M., Albarado, D.C., Redman, L.M., Bray, G.A., Noland, R.C., Munzberg, H., Hutson, S.M., Gettys, T.W., Schwartz, M.W., and Morrison, C.D. (2014). FGF21 is an endocrine signal of protein restriction. J Clin Invest *124*, 3913-3922. 10.1172/JCI74915.
56. Hill, C.M., Laeger, T., Dehner, M., Albarado, D.C., Clarke, B., Wanders, D., Burke, S.J., Collier, J.J., Qualls-Creekmore, E., Solon-Biet, S.M., et al. (2019). FGF21 Signals Protein Status to the Brain and Adaptively Regulates Food Choice and Metabolism. Cell reports *27*, 2934-2947 e2933. 10.1016/j.celrep.2019.05.022.
57. Fisher, F.M., Kleiner, S., Douris, N., Fox, E.C., Mepani, R.J., Verdeguer, F., Wu, J., Kharitonenkov, A., Flier, J.S., Maratos-Flier, E., and Spiegelman, B.M. (2012). FGF21 regulates PGC-1alpha and browning of white adipose tissues in adaptive thermogenesis. Genes Dev *26*, 271-281. 10.1101/gad.177857.111.
58. Hill, C.M., Laeger, T., Albarado, D.C., McDougal, D.H., Berthoud, H.R., Munzberg, H., and Morrison, C.D. (2017). Low protein-induced increases in FGF21 drive UCP1-dependent metabolic but not thermoregulatory endpoints. Scientific reports *7*, 8209. 10.1038/s41598-017-07498-w.
59. Minard, A.Y., Tan, S.X., Yang, P., Fazakerley, D.J., Domanova, W., Parker, B.L., Humphrey, S.J., Jothi, R., Stockli, J., and James, D.E. (2016). mTORC1 Is a Major Regulatory Node in the FGF21 Signaling Network in Adipocytes. Cell reports *17*, 29-36. 10.1016/j.celrep.2016.08.086.
60. Owen, B.M., Ding, X., Morgan, D.A., Coate, K.C., Bookout, A.L., Rahmouni, K., Kliewer, S.A., and Mangelsdorf, D.J. (2014). FGF21 acts centrally to induce sympathetic nerve activity, energy expenditure, and weight loss. Cell Metab *20*, 670-677. 10.1016/j.cmet.2014.07.012.
61. Miyake, M., Nomura, A., Ogura, A., Takehana, K., Kitahara, Y., Takahara, K., Tsugawa, K., Miyamoto, C., Miura, N., Sato, R., et al. (2016). Skeletal muscle-specific eukaryotic translation initiation factor 2alpha phosphorylation controls amino acid metabolism and

fibroblast growth factor 21-mediated non-cell-autonomous energy metabolism. FASEB J *30*, 798-812. 10.1096/fj.15-275990.
62. Schaap, F.G., Kremer, A.E., Lamers, W.H., Jansen, P.L.M., and Gaemers, I.C. (2013). Fibroblast growth factor 21 is induced by endoplasmic reticulum stress. Biochimie *95*, 692-699. https://doi.org/10.1016/j.biochi.2012.10.019.
63. Zarei, M., Barroso, E., Leiva, R., Barniol-Xicota, M., Pujol, E., Escolano, C., Vazquez, S., Palomer, X., Pardo, V., Gonzalez-Rodriguez, A., et al. (2016). Heme-Regulated eIF2alpha Kinase Modulates Hepatic FGF21 and Is Activated by PPARbeta/delta Deficiency. Diabetes *65*, 3185-3199. 10.2337/db16-0155.
64. Aon, M.A., Bernier, M., Mitchell, S.J., Di Germanio, C., Mattison, J.A., Ehrlich, M.R., Colman, R.J., Anderson, R.M., and de Cabo, R. (2020). Untangling Determinants of Enhanced Health and Lifespan through a Multi-omics Approach in Mice. Cell Metab *32*, 100-116 e104. 10.1016/j.cmet.2020.04.018.
65. Richardson, N.E., Konon, E.N., Schuster, H.S., Mitchell, A.T., Boyle, C., Rodgers, A.C., Finke, M., Haider, L.R., Yu, D., Flores, V., et al. (2021). Lifelong restriction of dietary branched-chain amino acids has sex-specific benefits for frailty and life span in mice. Nature Aging *1*, 73-86. 10.1038/s43587-020-00006-2.
66. Lamming, D.W., Cummings, N.E., Rastelli, A.L., Gao, F., Cava, E., Bertozzi, B., Spelta, F., Pili, R., and Fontana, L. (2015). Restriction of dietary protein decreases mTORC1 in tumors and somatic tissues of a tumor-bearing mouse xenograft model. Oncotarget *6*, 31233-31240. 10.18632/oncotarget.5180.
67. Calubag, M.F., Robbins, P.D., and Lamming, D.W. (2024). A nutrigeroscience approach: Dietary macronutrients and cellular senescence. Cell Metab *36*, 1914-1944. 10.1016/j.cmet.2024.07.025.
68. Lopez-Otin, C., Blasco, M.A., Partridge, L., Serrano, M., and Kroemer, G. (2013). The hallmarks of aging. Cell *153*, 1194-1217. 10.1016/j.cell.2013.05.039.
69. Carroll, B., Nelson, G., Rabanal-Ruiz, Y., Kucheryavenko, O., Dunhill-Turner, N.A., Chesterman, C.C., Zahari, Q., Zhang, T., Conduit, S.E., Mitchell, C.A., et al. (2017). Persistent mTORC1 signaling in cell senescence results from defects in amino acid and growth factor sensing. J Cell Biol *216*, 1949-1957. 10.1083/jcb.201610113.
70. Herranz, N., Gallage, S., Mellone, M., Wuestefeld, T., Klotz, S., Hanley, C.J., Raguz, S., Acosta, J.C., Innes, A.J., Banito, A., et al. (2015). mTOR regulates MAPKAPK2 translation to control the senescence-associated secretory phenotype. Nat Cell Biol *17*, 1205-1217. 10.1038/ncb3225.
71. Laberge, R.M., Sun, Y., Orjalo, A.V., Patil, C.K., Freund, A., Zhou, L., Curran, S.C., Davalos, A.R., Wilson-Edell, K.A., Liu, S., et al. (2015). MTOR regulates the pro-tumorigenic senescence-associated secretory phenotype by promoting IL1A translation. Nat Cell Biol *17*, 1049-1061. 10.1038/ncb3195.
72. Nakano, M., Nakashima, A., Nagano, T., Ishikawa, S., Kikkawa, U., and Kamada, S. (2013). Branched-Chain Amino Acids Enhance Premature Senescence through Mammalian Target of Rapamycin Complex I-Mediated Upregulation of p21 Protein. PLOS ONE *8*, e80411. 10.1371/journal.pone.0080411.
73. Tournissac, M., Vandal, M., Tremblay, C., Bourassa, P., Vancassel, S., Emond, V., Gangloff, A., and Calon, F. (2018). Dietary intake of branched-chain amino acids in a mouse model of Alzheimer's disease: Effects on survival, behavior, and neuropathology. Alzheimers Dement (N Y) *4*, 677-687. 10.1016/j.trci.2018.10.005.
74. Ritzel, R.M., Doran, S.J., Glaser, E.P., Meadows, V.E., Faden, A.I., Stoica, B.A., and Loane, D.J. (2019). Old age increases microglial senescence, exacerbates secondary

neuroinflammation, and worsens neurological outcomes after acute traumatic brain injury in mice. Neurobiol Aging *77*, 194-206. 10.1016/j.neurobiolaging.2019.02.010.
75. Sparkman, N.L., and Johnson, R.W. (2008). Neuroinflammation associated with aging sensitizes the brain to the effects of infection or stress. Neuroimmunomodulation *15*, 323-330. 10.1159/000156474.
76. Zhang, W., Xiao, D., Mao, Q., and Xia, H. (2023). Role of neuroinflammation in neurodegeneration development. Signal Transduction and Targeted Therapy *8*, 267. 10.1038/s41392-023-01486-5.
77. Ownby, R.L. (2010). Neuroinflammation and cognitive aging. Curr Psychiatry Rep *12*, 39-45. 10.1007/s11920-009-0082-1.
78. Liu, T.T., Thomas, S., McLean, D.T., Roldan-Alzate, A., Hernando, D., Ricke, E.A., and Ricke, W.A. (2019). Prostate enlargement and altered urinary function are part of the aging process. Aging (Albany NY) *11*, 2653-2669. 10.18632/aging.101938.
79. Ligon, M.M., Joshi, C.S., Fashemi, B.E., Salazar, A.M., and Mysorekar, I.U. (2023). Effects of aging on urinary tract epithelial homeostasis and immunity. Developmental Biology *493*, 29-39. https://doi.org/10.1016/j.ydbio.2022.11.003.
80. Brayton, C.F., Treuting, P.M., and Ward, J.M. (2012). Pathobiology of Aging Mice and GEM: Background Strains and Experimental Design. Veterinary Pathology *49*, 85-105. 10.1177/0300985811430696.
81. Blackwell, B.N., Bucci, T.J., Hart, R.W., and Turturro, A. (1995). Longevity, body weight, and neoplasia in ad libitum-fed and diet-restricted C57BL6 mice fed NIH-31 open formula diet. Toxicologic pathology *23*, 570-582. 10.1177/019262339502300503.
82. Brandhorst, S., Choi, I.Y., Wei, M., Cheng, C.W., Sedrakyan, S., Navarrete, G., Dubeau, L., Yap, L.P., Park, R., Vinciguerra, M., et al. (2015). A Periodic Diet that Mimics Fasting Promotes Multi-System Regeneration, Enhanced Cognitive Performance, and Healthspan. Cell Metab *22*, 86-99. 10.1016/j.cmet.2015.05.012.
83. Strong, R., Miller, R.A., Antebi, A., Astle, C.M., Bogue, M., Denzel, M.S., Fernandez, E., Flurkey, K., Hamilton, K.L., Lamming, D.W., et al. (2016). Longer lifespan in male mice treated with a weakly estrogenic agonist, an antioxidant, an alpha-glucosidase inhibitor or a Nrf2-inducer. Aging Cell *15*, 872-884. 10.1111/acel.12496.
84. Barcena, C., Quiros, P.M., Durand, S., Mayoral, P., Rodriguez, F., Caravia, X.M., Marino, G., Garabaya, C., Fernandez-Garcia, M.T., Kroemer, G., et al. (2018). Methionine Restriction Extends Lifespan in Progeroid Mice and Alters Lipid and Bile Acid Metabolism. Cell reports *24*, 2392-2403. 10.1016/j.celrep.2018.07.089.
85. Kosakamoto, H., Obata, F., Kuraishi, J., Aikawa, H., Okada, R., Johnstone, J.N., Onuma, T., Piper, M.D.W., and Miura, M. (2023). Early-adult methionine restriction reduces methionine sulfoxide and extends lifespan in Drosophila. Nature Communications *14*, 7832. 10.1038/s41467-023-43550-2.
86. Lee, B.C., Kaya, A., Ma, S., Kim, G., Gerashchenko, M.V., Yim, S.H., Hu, Z., Harshman, L.G., and Gladyshev, V.N. (2014). Methionine restriction extends lifespan of Drosophila melanogaster under conditions of low amino-acid status. Nature Communications *5*, 3592. 10.1038/ncomms4592.
87. Parkhitko, A.A., Wang, L., Filine, E., Jouandin, P., Leshchiner, D., Binari, R., Asara, J.M., Rabinowitz, J.D., and Perrimon, N. (2021). A genetic model of methionine restriction extends Drosophila health- and lifespan. Proc Natl Acad Sci U S A *118*. 10.1073/pnas.2110387118.
88. Richie, J.P., Jr., Leutzinger, Y., Parthasarathy, S., Malloy, V., Orentreich, N., and Zimmerman, J.A. (1994). Methionine restriction increases blood glutathione and longevity in F344 rats. FASEB J *8*, 1302-1307. 10.1096/fasebj.8.15.8001743.

89. Sun, L., Sadighi Akha, A.A., Miller, R.A., and Harper, J.M. (2009). Life-span extension in mice by preweaning food restriction and by methionine restriction in middle age. J Gerontol A Biol Sci Med Sci *64*, 711-722. 10.1093/gerona/glp051.
90. Yu, D., Yang, S.E., Miller, B.R., Wisinski, J.A., Sherman, D.S., Brinkman, J.A., Tomasiewicz, J.L., Cummings, N.E., Kimple, M.E., Cryns, V.L., and Lamming, D.W. (2018). Short-term methionine deprivation improves metabolic health via sexually dimorphic, mTORC1-independent mechanisms. FASEB J *32*, 3471-3482. 10.1096/fj.201701211R.
91. Forney, L.A., Fang, H., Sims, L.C., Stone, K.P., Vincik, L.Y., Vick, A.M., Gibson, A.N., Burk, D.H., and Gettys, T.W. (2020). Dietary Methionine Restriction Signals to the Brain Through Fibroblast Growth Factor 21 to Regulate Energy Balance and Remodeling of Adipose Tissue. Obesity (Silver Spring) *28*, 1912-1921. 10.1002/oby.22919.
92. Kitada, M., Xu, J., Ogura, Y., Monno, I., and Koya, D. (2020). Mechanism of Activation of Mechanistic Target of Rapamycin Complex 1 by Methionine. Front Cell Dev Biol *8*, 715. 10.3389/fcell.2020.00715.
93. Aman, Y., Schmauck-Medina, T., Hansen, M., Morimoto, R.I., Simon, A.K., Bjedov, I., Palikaras, K., Simonsen, A., Johansen, T., Tavernarakis, N., et al. (2021). Autophagy in healthy aging and disease. Nature Aging *1*, 634-650. 10.1038/s43587-021-00098-4.
94. Hansen, M., Rubinsztein, D.C., and Walker, D.W. (2018). Autophagy as a promoter of longevity: insights from model organisms. Nat Rev Mol Cell Biol *19*, 579-593. 10.1038/s41580-018-0033-y.
95. Madeo, F., Zimmermann, A., Maiuri, M.C., and Kroemer, G. (2015). Essential role for autophagy in life span extension. J Clin Invest *125*, 85-93. 10.1172/JCI73946.
96. Markaki, M., Metaxakis, A., and Tavernarakis, N. (2017). Chapter 2 - The Role of Autophagy in Aging: Molecular Mechanisms. In Autophagy: Cancer, Other Pathologies, Inflammation, Immunity, Infection, and Aging, M.A. Hayat, ed. (Academic Press), pp. 123-138. https://doi.org/10.1016/B978-0-12-812146-7.00002-0.
97. Hochmuth, L., Korner, C., Ott, F., Volke, D., Cokan, K.B., Juvan, P., Brosch, M., Hofmann, U., Hoffmann, R., Rozman, D., et al. (2021). Sex-dependent dynamics of metabolism in primary mouse hepatocytes. Arch Toxicol *95*, 3001-3013. 10.1007/s00204-021-03118-9.
98. Costanzo, M., Caterino, M., Sotgiu, G., Ruoppolo, M., Franconi, F., and Campesi, I. (2022). Sex differences in the human metabolome. Biol Sex Differ *13*, 30. 10.1186/s13293-022-00440-4.
99. Mora, S., Mann, G., and Adegoke, O.A.J. (2024). Sex differences in cachexia and branched-chain amino acid metabolism following chemotherapy in mice. Physiol Rep *12*, e16003. 10.14814/phy2.16003.
100. Schultz, M.B., Kane, A.E., Mitchell, S.J., MacArthur, M.R., Warner, E., Vogel, D.S., Mitchell, J.R., Howlett, S.E., Bonkowski, M.S., and Sinclair, D.A. (2020). Age and life expectancy clocks based on machine learning analysis of mouse frailty. Nature communications *11*, 4618. 10.1038/s41467-020-18446-0.
101. Kane, A.E., Gregson, E., Theou, O., Rockwood, K., and Howlett, S.E. (2017). The association between frailty, the metabolic syndrome, and mortality over the lifespan. Geroscience *39*, 221-229. 10.1007/s11357-017-9967-9.
102. Rockwood, K., Blodgett, J.M., Theou, O., Sun, M.H., Feridooni, H.A., Mitnitski, A., Rose, R.A., Godin, J., Gregson, E., and Howlett, S.E. (2017). A Frailty Index Based On Deficit Accumulation Quantifies Mortality Risk in Humans and in Mice. Scientific reports *7*, 43068. 10.1038/srep43068.
103. Bjune, M.S., Lawrence-Archer, L., Laupsa-Borge, J., Sommersten, C.H., McCann, A., Glastad, R.C., Johnston, I.G., Kern, M., Bluher, M., Mellgren, G., and Dankel, S.N. (2023).

Metabolic role of the hepatic valine/3-hydroxyisobutyrate (3-HIB) pathway in fatty liver disease. EBioMedicine *91*, 104569. 10.1016/j.ebiom.2023.104569.
104. Jian, H., Miao, S., Liu, Y., Wang, X., Xu, Q., Zhou, W., Li, H., Dong, X., and Zou, X. (2021). Dietary Valine Ameliorated Gut Health and Accelerated the Development of Nonalcoholic Fatty Liver Disease of Laying Hens. Oxid Med Cell Longev *2021*, 4704771. 10.1155/2021/4704771.
105. Shi, X., Yin, H., Li, J., Huang, C., Chen, Y., Chen, Z., Liu, W., Weijuan, S., Zhang, Y., Lin, M., et al. (2021). Circulating branch chain amino acids and improvement in liver fat content in response to exercise interventions in NAFLD. Scientific Reports *11*, 13415. 10.1038/s41598-021-92918-1.
106. Yang, X., Schadt, E.E., Wang, S., Wang, H., Arnold, A.P., Ingram-Drake, L., Drake, T.A., and Lusis, A.J. (2006). Tissue-specific expression and regulation of sexually dimorphic genes in mice. Genome Res *16*, 995-1004. 10.1101/gr.5217506.
107. Joshi, J.N., Lerner, A.D., Scallo, F., Grumet, A.N., Matteson, P., Millonig, J.H., and Valvezan, A.J. (2024). mTORC1 activity oscillates throughout the cell cycle, promoting mitotic entry and differentially influencing autophagy induction. Cell Rep *43*, 114543. 10.1016/j.celrep.2024.114543.
108. Abdellatif, M., Eisenberg, T., Heberle, A.M., Thedieck, K., Kroemer, G., and Sedej, S. (2022). Cardiac PI3K p110alpha attenuation delays aging and extends lifespan. Cell Stress *6*, 72-75. 10.15698/cst2022.08.270.
109. Hedges, C.P., Shetty, B., Broome, S.C., MacRae, C., Koutsifeli, P., Buckels, E.J., MacIndoe, C., Boix, J., Tsiloulis, T., Matthews, B.G., et al. (2023). Dietary supplementation of clinically utilized PI3K p110alpha inhibitor extends the lifespan of male and female mice. Nat Aging *3*, 162-172. 10.1038/s43587-022-00349-y.
110. Liu, Y., Liu, Q., Zhang, Z., Yang, Y., Zhou, Y., Yan, H., Wang, X., Li, X., Zhao, J., Hu, J., et al. (2023). The regulatory role of PI3K in ageing-related diseases. Ageing Res Rev *88*, 101963. 10.1016/j.arr.2023.101963.
111. Lopez-Guadamillas, E., Munoz-Martin, M., Martinez, S., Pastor, J., Fernandez-Marcos, P.J., and Serrano, M. (2016). PI3Kalpha inhibition reduces obesity in mice. Aging (Albany NY) *8*, 2747-2753. 10.18632/aging.101075.
112. Okuyama, T., Inoue, H., Ookuma, S., Satoh, T., Kano, K., Honjoh, S., Hisamoto, N., Matsumoto, K., and Nishida, E. (2010). The ERK-MAPK pathway regulates longevity through SKN-1 and insulin-like signaling in Caenorhabditis elegans. J Biol Chem *285*, 30274-30281. 10.1074/jbc.M110.146274.
113. Troemel, E.R., Chu, S.W., Reinke, V., Lee, S.S., Ausubel, F.M., and Kim, D.H. (2006). p38 MAPK regulates expression of immune response genes and contributes to longevity in C. elegans. PLoS Genet *2*, e183. 10.1371/journal.pgen.0020183.
114. Yuan, W., Weaver, Y.M., Earnest, S., Taylor, C.A., Cobb, M.H., and Weaver, B.P. (2023). Modulating p38 MAPK signaling by proteostasis mechanisms supports tissue integrity during growth and aging. Nature Communications *14*, 4543. 10.1038/s41467-023-40317-7.
115. Kennedy, B.K., and Lamming, D.W. (2016). The Mechanistic Target of Rapamycin: The Grand ConducTOR of Metabolism and Aging. Cell Metab *23*, 990-1003. 10.1016/j.cmet.2016.05.009.
116. Dorman, J.B., Albinder, B., Shroyer, T., and Kenyon, C. (1995). The age-1 and daf-2 genes function in a common pathway to control the lifespan of Caenorhabditis elegans. Genetics *141*, 1399-1406. 10.1093/genetics/141.4.1399.
117. Kenyon, C., Chang, J., Gensch, E., Rudner, A., and Tabtiang, R. (1993). A C. elegans mutant that lives twice as long as wild type. Nature *366*, 461-464. 10.1038/366461a0.

118. Calubag, M.F., Ademi, I., Grunow, I.D., Breuer, L.E., Babygirija, R., Lialios, P., Le, S.M., Sonsalla, M.M., Illiano, J.A., Knopf, B.A., et al. (2025). Tissue-Specific Effects of Dietary Protein on Cellular Senescence Are Mediated by Branched-Chain Amino Acids. Aging Cell, e70176. 10.1111/acel.70176.
119. Song, J., Sun, J., Jing, S., Zhang, T., Wang, J., and Liu, Y. (2023). A high level of secreted phosphoprotein 1 is associated with macrophage infiltration and poor prognosis in hepatocellular carcinoma. ILIVER *2*, 26-35. 10.1016/j.iliver.2023.01.004.
120. Song, Z., Chen, W., Athavale, D., Ge, X., Desert, R., Das, S., Han, H., and Nieto, N. (2021). Osteopontin Takes Center Stage in Chronic Liver Disease. Hepatology *73*, 1594-1608. 10.1002/hep.31582.
121. Moreno-Viedma, V., Tardelli, M., Zeyda, M., Sibilia, M., Burks, J.D., and Stulnig, T.M. (2018). Osteopontin-deficient progenitor cells display enhanced differentiation to adipocytes. Obes Res Clin Pract *12*, 277-285. 10.1016/j.orcp.2018.02.006.
122. Sawaki, D., Zhang, Y., Mohamadi, A., Pini, M., Mezdari, Z., Lipskaia, L., Naushad, S., Lamendour, L., Altintas, D.M., Breau, M., et al. (2023). Osteopontin promotes age-related adipose tissue remodeling through senescence-associated macrophage dysfunction. JCI Insight *8*. 10.1172/jci.insight.145811.
123. Bi, W., Yang, M., Shi, M., Hou, M., Jiang, C., Fan, G., and Guo, W. (2024). A comprehensive single-cell RNA transcriptomic analysis identifies a unique SPP1+ macrophages subgroup in aging skeletal muscle. Sci Rep *14*, 18156. 10.1038/s41598-024-69284-9.
124. Farahat, P.K., Kumagai-Cresse, C., Aragon, R.L., Ma, F., Amakor, J.K., Espinoza, A., Kramerova, I., Jimenez, R.J., Smith, B.M., Perez, J., et al. (2025). Macrophage-derived Spp1 promotes intramuscular fat in dystrophic muscle. JCI Insight *10*. 10.1172/jci.insight.181946.
125. Cha, S.M., Park, J.W., Lee, Y.J., Lee, H.J., Lee, H., Lee, I.W., Gong, G., Park, S.H., Lee, H.J., and Jeong, B.K. (2024). SPP1+ macrophages in HR+ breast cancer are associated with tumor-infiltrating lymphocytes. NPJ Breast Cancer *10*, 83. 10.1038/s41523-024-00695-7.
126. Liu, C., Wu, K., Li, C., Zhang, Z., Zhai, P., Guo, H., and Zhang, J. (2024). SPP1+ macrophages promote head and neck squamous cell carcinoma progression by secreting TNF-alpha and IL-1beta. J Exp Clin Cancer Res *43*, 332. 10.1186/s13046-024-03255-w.
127. Trehan, R., Huang, P., Zhu, X.B., Wang, X., Soliman, M., Strepay, D., Nur, A., Kedei, N., Arhin, M., Ghabra, S., et al. (2025). SPP1 + macrophages cause exhaustion of tumor-specific T cells in liver metastases. Nat Commun *16*, 4242. 10.1038/s41467-025-59529-0.
128. Wang, H., Qiu, B., Li, X., Ying, Y., Wang, Y., Chen, H., Zeng, F., Shi, J., Huang, J., Wu, Z., et al. (2025). Single cell analysis reveals that SPP1(+) macrophages enhance tumor progression by triggering fibroblast extracellular vesicles. Transl Oncol *55*, 102347. 10.1016/j.tranon.2025.102347.
129. Solon-Biet, S.M., McMahon, A.C., Ballard, J.W., Ruohonen, K., Wu, L.E., Cogger, V.C., Warren, A., Huang, X., Pichaud, N., Melvin, R.G., et al. (2014). The ratio of macronutrients, not caloric intake, dictates cardiometabolic health, aging, and longevity in ad libitum-fed mice. Cell Metab *19*, 418-430. 10.1016/j.cmet.2014.02.009.
130. Mitchell, S.J., Madrigal-Matute, J., Scheibye-Knudsen, M., Fang, E., Aon, M., Gonzalez-Reyes, J.A., Cortassa, S., Kaushik, S., Gonzalez-Freire, M., Patel, B., et al. (2016). Effects of Sex, Strain, and Energy Intake on Hallmarks of Aging in Mice. Cell Metab *23*, 1093-1112. 10.1016/j.cmet.2016.05.027.
131. Weindruch, R., Walford, R.L., Fligiel, S., and Guthrie, D. (1986). The retardation of aging in mice by dietary restriction: longevity, cancer, immunity and lifetime energy intake. The Journal of nutrition *116*, 641-654. 10.1093/jn/116.4.641.

132. Miller, R.A., Harrison, D.E., Astle, C.M., Fernandez, E., Flurkey, K., Han, M., Javors, M.A., Li, X., Nadon, N.L., Nelson, J.F., et al. (2014). Rapamycin-mediated lifespan increase in mice is dose and sex dependent and metabolically distinct from dietary restriction. Aging Cell *13*, 468-477. 10.1111/acel.12194.
133. Liao, C.Y., Rikke, B.A., Johnson, T.E., Diaz, V., and Nelson, J.F. (2010). Genetic variation in the murine lifespan response to dietary restriction: from life extension to life shortening. Aging Cell *9*, 92-95. 10.1111/j.1474-9726.2009.00533.x.

Figure 1

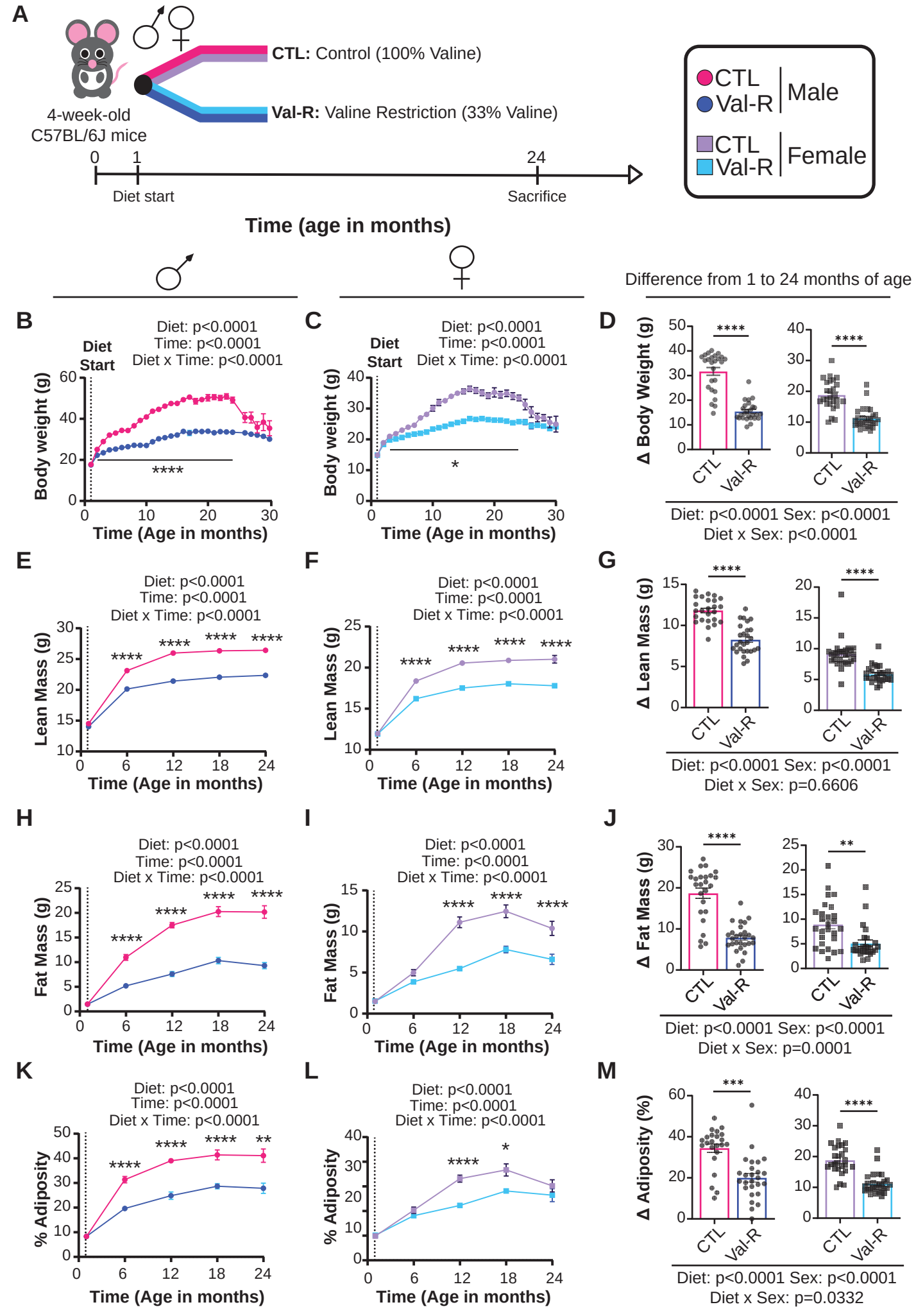
A
4-week-old
C57BL/6J mice
CTL: Control (100% Valine)
Val-R: Valine Restriction (33% Valine)
0
1
24
Diet start
Sacrifice
Time (age in months)
CTL
Val-R
Male
CTL
Val-R
Female
Difference from 1 to 24 months of age
B
Diet: p<0.0001
Time: p<0.0001
Diet x Time: p<0.0001
Diet Start
Body weight (g)
Time (Age in months)
C
Diet: p<0.0001
Time: p<0.0001
Diet x Time: p<0.0001
Diet Start
Body weight (g)
Time (Age in months)
D
Δ Body Weight (g)
CTL
Val-R
Diet: p<0.0001 Sex: p<0.0001
Diet x Sex: p<0.0001
E
Diet: p<0.0001
Time: p<0.0001
Diet x Time: p<0.0001
Lean Mass (g)
Time (Age in months)
F
Diet: p<0.0001
Time: p<0.0001
Diet x Time: p<0.0001
Lean Mass (g)
Time (Age in months)
G
Δ Lean Mass (g)
CTL
Val-R
Diet: p<0.0001 Sex: p<0.0001
Diet x Sex: p=0.6606
H
Diet: p<0.0001
Time: p<0.0001
Diet x Time: p<0.0001
Fat Mass (g)
Time (Age in months)
I
Diet: p<0.0001
Time: p<0.0001
Diet x Time: p<0.0001
Fat Mass (g)
Time (Age in months)
J
Δ Fat Mass (g)
CTL
Val-R
Diet: p<0.0001 Sex: p<0.0001
Diet x Sex: p=0.0001
K
Diet: p<0.0001
Time: p<0.0001
Diet x Time: p<0.0001
% Adiposity
Time (Age in months)
L
Diet: p<0.0001
Time: p<0.0001
Diet x Time: p<0.0001
% Adiposity
Time (Age in months)
M
Δ Adiposity (%)
CTL
Val-R
Diet: p<0.0001 Sex: p<0.0001
Diet x Sex: p=0.0332

Figure Legends

Figure 1: Val-R attenuates body weight and fat mass accretion in both males and females.

(A) Experimental design. (B-D) Body weight of male (B) and female (C) mice over 30 months and change in body weight from 1 month of age until 24 months of age (D). (E-G) Lean mass of male (E) and female (F) mice over 30 months and change in lea mass from 1 month of age until 24 months of age (G). (H-J) Fat mass of male (H) and female (I) mice over 30 months and change in body weight from 1 month of age until 24 months of age (J). (K-M) Percent adiposity of male (K) and female (L) mice over 30 months and change in body weight from 1 month of age until 24 months of age (M). (B-M) n=37 mice/group; two-way ANOVA, *$p<0.05$, **$p<0.01$, ***$p<0.001$, ****$p<0.0001$; statistics for the overall effects of time, diet, and the interaction represent the p value from a two-way ANOVA. Data represented as mean ± SEM.

Figure 2

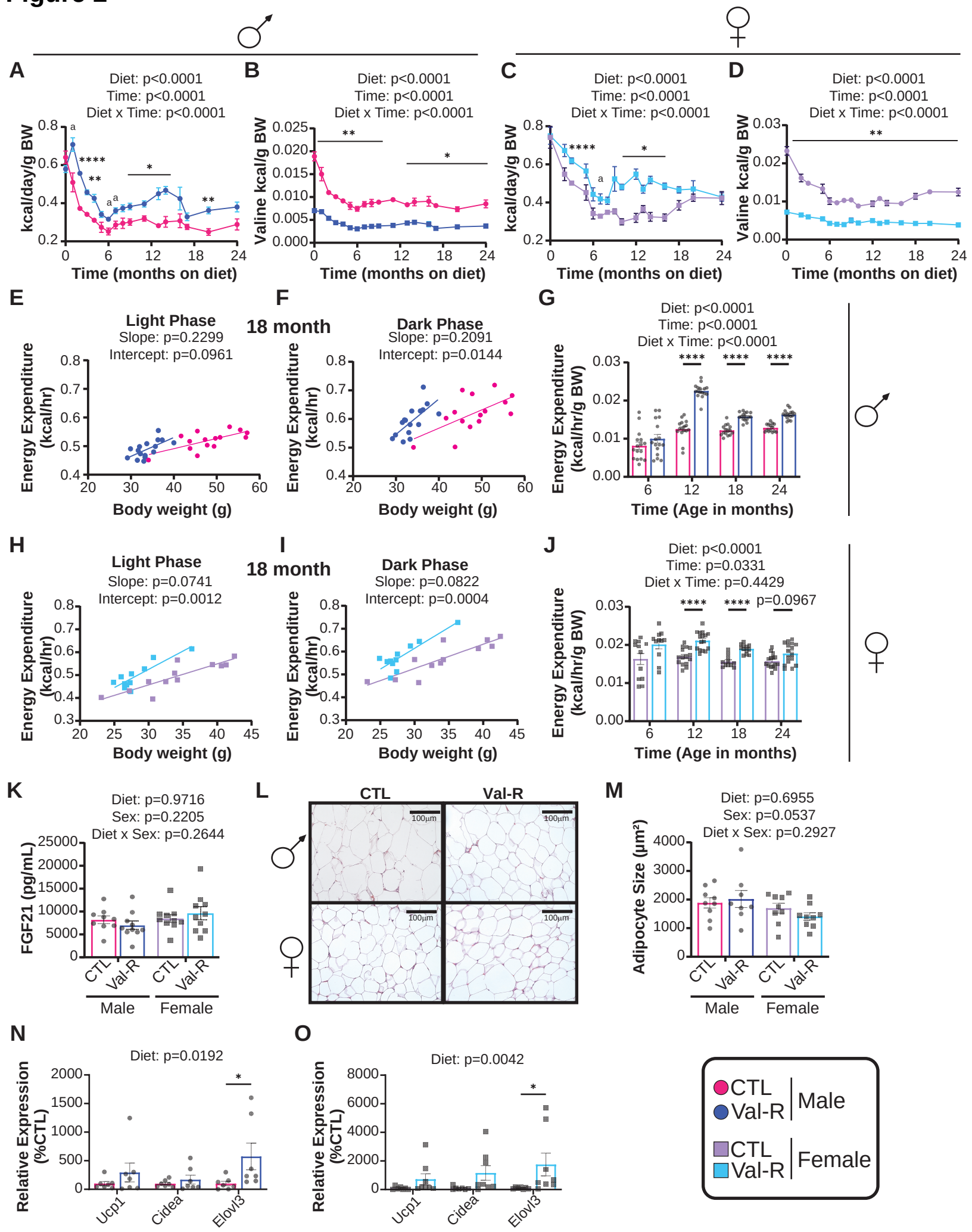
A
Diet: p<0.0001
Time: p<0.0001
Diet x Time: p<0.0001
kcal/day/g BW
Time (months on diet)
B
Diet: p<0.0001
Time: p<0.0001
Diet x Time: p<0.0001
Valine kcal/g BW
Time (months on diet)
C
Diet: p<0.0001
Time: p<0.0001
Diet x Time: p<0.0001
kcal/day/g BW
Time (months on diet)
D
Diet: p<0.0001
Time: p<0.0001
Diet x Time: p<0.0001
Valine kcal/g BW
Time (months on diet)
E
Light Phase
Slope: p=0.2299
Intercept: p=0.0961
Energy Expenditure (kcal/hr)
Body weight (g)
F
18 month
Dark Phase
Slope: p=0.2091
Intercept: p=0.0144
Energy Expenditure (kcal/hr)
Body weight (g)
G
Diet: p<0.0001
Time: p<0.0001
Diet x Time: p<0.0001
Energy Expenditure (kcal/hr/g BW)
Time (Age in months)
H
Light Phase
Slope: p=0.0741
Intercept: p=0.0012
Energy Expenditure (kcal/hr)
Body weight (g)
I
18 month
Dark Phase
Slope: p=0.0822
Intercept: p=0.0004
Energy Expenditure (kcal/hr)
Body weight (g)
J
Diet: p<0.0001
Time: p=0.0331
Diet x Time: p=0.4429
p=0.0967
Energy Expenditure (kcal/hr/g BW)
Time (Age in months)
K
Diet: p=0.9716
Sex: p=0.2205
Diet x Sex: p=0.2644
FGF21 (pg/mL)
CTL
Val-R
Male
Female
L
CTL
Val-R
100µm
M
Diet: p=0.6955
Sex: p=0.0537
Diet x Sex: p=0.2927
Adipocyte Size (µm²)
CTL
Val-R
Male
Female
N
Diet: p=0.0192
Relative Expression (%CTL)
Ucp1
Cidea
Elovl3
O
Diet: p=0.0042
Relative Expression (%CTL)
Ucp1
Cidea
Elovl3
CTL
Val-R
Male
CTL
Val-R
Female

Figure 2: Val-R increases energy expenditure via the induction of thermogenesis in iWAT.

(A) Kilocalorie intake per day per gram of body weight (kcal/day/g BW) measured over 24 months on diet in males (n=4-20 mice/group). (B) Kilocalories derived from valine per gram of body weight (Valine kcal/g BW) over 24 months on diet in males (n=4-20 mice/group). (C-D) Kcal/day/g BW (C) and Valine kcal/g BW (D) over 24 months on diet in female mice (n=4-20 mice/group). (E-F) Energy expenditure of male mice as a function of body weight in the light (E) and dark (F) phase (n=15-16 mice/group). (G) Average energy expenditure normalized to body weight at 6, 12, 18 and 24 months of age in male mice (n=14-16 mice/group). (H-I) Energy expenditure of female mice as a function of body weight in the light (H) and dark (I) phase (n=11-12 mice/group). (J) Average energy expenditure normalized to body weight at 6, 12, 18 and 24 months of age in female mice (n=14-16 mice/group). (K) Circulating FGF21 at 19 months of age. (n=10-12 mice/group) (L) Hematoxylin and eosin (HE) staining (representative images; scale bar=100μm, 40X magnification) from iWAT of male and female mice. (M) Quantified adipocyte size (μm^2) from HE-stained iWAT images from male mice (n=6-9 mice/group). (N-O) The mRNA expression of three lipogenic genes *Ucp1, Cidea,* and *Elovl3*, was quantified in the iWAT of male (N) and female (O) mice (n=7-8 mice/group). (A-D, G, J) statistics for the overall effects of time, diet, and the interaction represent the p value from a two-way RM ANOVA or REML analysis. (E-F, H-I) data for each individual mouse is plotted; simple linear regression (ANCOVA) was calculated to determine if the slopes or elevations are equal; if the slopes are significantly different, differences in elevation cannot be determined. (K, M) statistics for the overall effects of sex, diet, and the interaction represent the p value from a two-way ANOVA. (N-O) statistics for the overall effects of gene, diet, and the interaction represent the p value from a two-way ANOVA. (A-D, G, J, K, M-O) a=p<0.1, *p<0.05, **p<0.01, ****p<0.0001 from a Sidak's post-test examining the effect of parameters identified as significant in the 2-way ANOVA. Data represented as mean ± SEM.

Figure 3

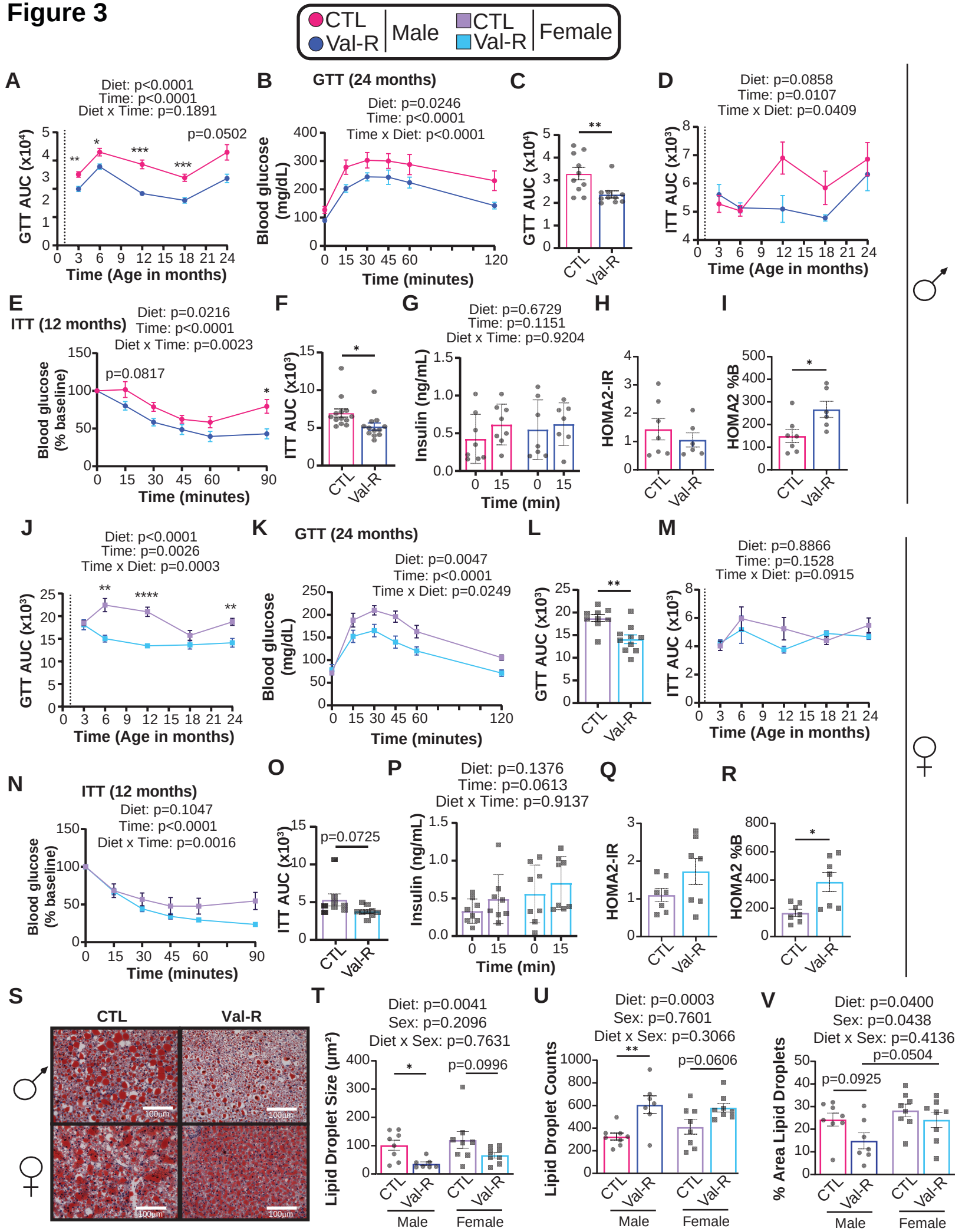
CTL
Val-R
Male
CTL
Val-R
Female
A
Diet: p<0.0001
Time: p<0.0001
Diet x Time: p=0.1891
p=0.0502
GTT AUC (x10⁴)
Time (Age in months)
B
GTT (24 months)
Diet: p=0.0246
Time: p<0.0001
Time x Diet: p<0.0001
Blood glucose (mg/dL)
Time (minutes)
C
GTT AUC (x10⁴)
D
Diet: p=0.0858
Time: p=0.0107
Time x Diet: p=0.0409
ITT AUC (x10³)
Time (Age in months)
E
ITT (12 months)
Diet: p=0.0216
Time: p<0.0001
Diet x Time: p=0.0023
p=0.0817
Blood glucose (% baseline)
Time (minutes)
F
ITT AUC (x10³)
G
Diet: p=0.6729
Time: p=0.1151
Diet x Time: p=0.9204
Insulin (ng/mL)
Time (min)
H
HOMA2-IR
I
HOMA2 %B
J
Diet: p<0.0001
Time: p=0.0026
Time x Diet: p=0.0003
GTT AUC (x10³)
Time (Age in months)
K
GTT (24 months)
Diet: p=0.0047
Time: p<0.0001
Time x Diet: p=0.0249
Blood glucose (mg/dL)
Time (minutes)
L
GTT AUC (x10³)
M
Diet: p=0.8866
Time: p=0.1528
Time x Diet: p=0.0915
ITT AUC (x10³)
Time (Age in months)
N
ITT (12 months)
Diet: p=0.1047
Time: p<0.0001
Diet x Time: p=0.0016
Blood glucose (% baseline)
Time (minutes)
O
ITT AUC (x10³)
p=0.0725
P
Diet: p=0.1376
Time: p=0.0613
Diet x Time: p=0.9137
Insulin (ng/mL)
Time (min)
Q
HOMA2-IR
R
HOMA2 %B
S
CTL
Val-R
100µm
T
Diet: p=0.0041
Sex: p=0.2096
Diet x Sex: p=0.7631
p=0.0996
Lipid Droplet Size (µm²)
Male
Female
U
Diet: p=0.0003
Sex: p=0.7601
Diet x Sex: p=0.3066
p=0.0606
Lipid Droplet Counts
Male
Female
V
Diet: p=0.0400
Sex: p=0.0438
Diet x Sex: p=0.4136
p=0.0504
p=0.0925
% Area Lipid Droplets
Male
Female

Figure 3: Val-R improves glucose regulation and protects form hepatic steatosis.

(A) Glucose tolerance area under the curve (GTT AUC) over time in male mice (n=11-12 mice/group). (B-C) A glucose tolerance test (B) performed at 24 months of age and its GTT AUC (C) in male mice (n=11-12 mice/group). (D) Insulin tolerance area under the curve (ITT AUC) over time in male mice (n=9-13 mice/group). (E-F) An insulin tolerance test (E) performed at 12 months of age and its ITT AUC (F) in male mice (n=12-13 mice/group). (G) A glucose stimulated insulin secretion (GSIS) assay performed at 19 months of age (n=8 mice/group). (H-I) HOMA2-IR (H) and HOMA2 %B (I) calculated at 19 months of age in male mice (n=6-7 mice/group). (J) GTT AUC over time in female mice. (K-L) A GTT (K) performed at 24 months of age and its GTT AUC (L) in female mice (n=9-12 mice/group). (M) ITT AUC over time in female mice (n=8-12 mice/group). (N-O) An ITT (N) performed at 12 months of age and its ITT AUC (O) in female mice (n=9 mice/group). (P) A GSIS assay performed at 19 months of age (n=8 mice/group). (Q-R) HOMA2-IR (Q) and HOMA2 %B (R) calculated at 19 months of age in female mice (n=7-8 mice/group). (S) Oil-Red-O (ORO) staining (representative images; scale bar=100μm, 40X magnification) from the liver of male and female mice (n=7-8 mice/group). (T-U) Quantified lipid droplet size (μm^2) (T), lipid droplet count (U), and percent of area of lipid droplets calculated from ORO-stained liver images (n=7-8 mice/group). (A-B, D-E, G, J-K, M-N, P) statistics for the overall effects of time, diet, and the interaction represent the p value from a two-way RM ANOVA analysis. (C, F, H-I, L, O, Q-R) Student's t-test. (T-V) statistics for the overall effects of sex, diet, and the interaction represent the p value from a two-way ANOVA. (A-R, T-V) *$p<0.05$, **$p<0.01$, ****$p<0.0001$ from a Sidak's post-test examining the effect of parameters identified as significant in the 2-way ANOVA or student's t-test. Data represented as mean ± SEM.

Figure 4

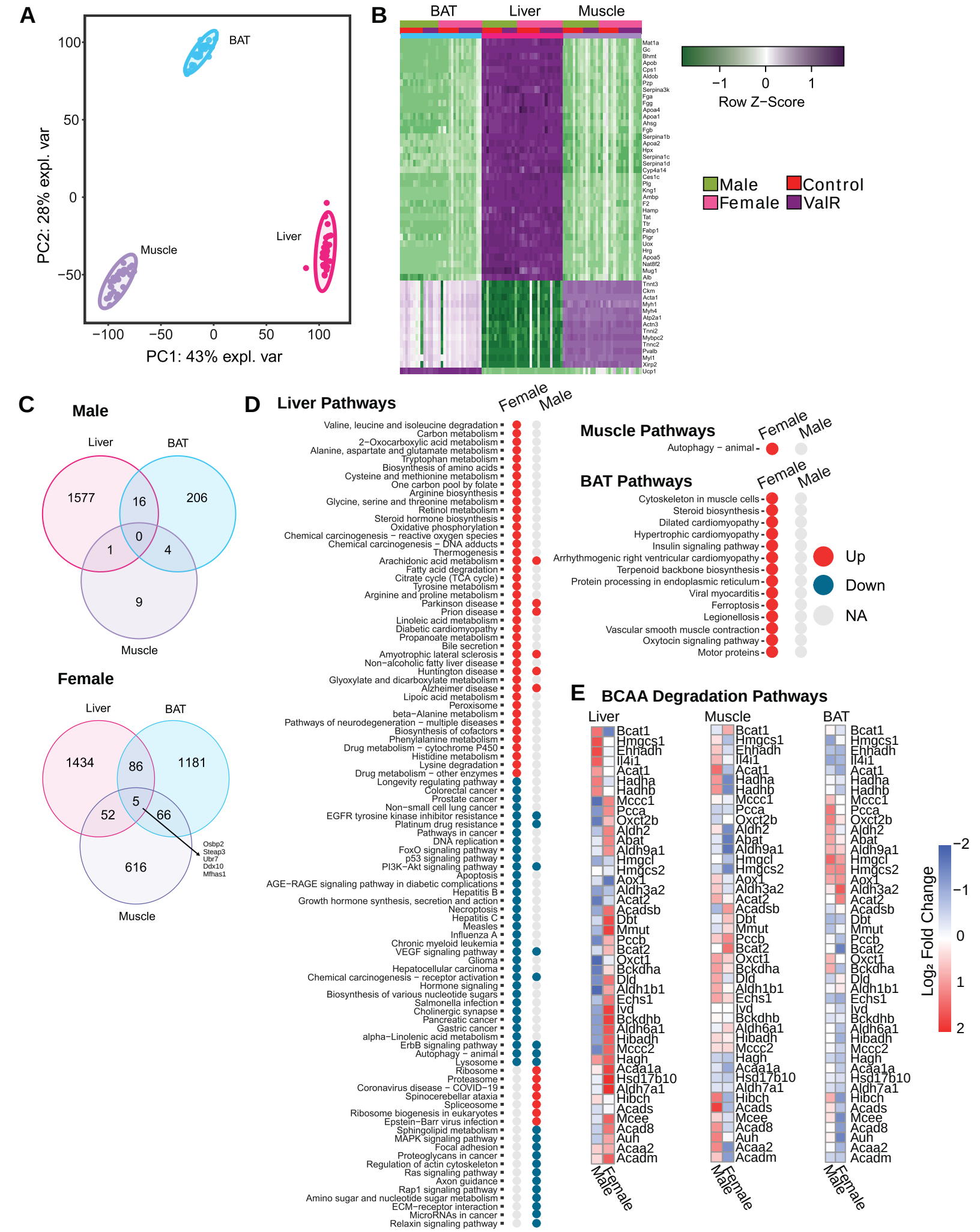
A
BAT
Liver
Muscle
PC2: 28% expl. var
PC1: 43% expl. var
B
BAT
Liver
Muscle
Row Z−Score
Male
Female
Control
ValR
C
Male
Liver
BAT
Muscle
1577
16
206
0
1
4
9
Female
Liver
BAT
Muscle
1434
86
1181
5
52
66
616
Osbp2
Steap3
Ubr7
Ddx10
Mfhas1
D
Liver Pathways
Female
Male
Muscle Pathways
Autophagy − animal
BAT Pathways
Cytoskeleton in muscle cells
Steroid biosynthesis
Dilated cardiomyopathy
Hypertrophic cardiomyopathy
Insulin signaling pathway
Arrhythmogenic right ventricular cardiomyopathy
Terpenoid backbone biosynthesis
Protein processing in endoplasmic reticulum
Viral myocarditis
Ferroptosis
Legionellosis
Vascular smooth muscle contraction
Oxytocin signaling pathway
Motor proteins
Up
Down
NA
E
BCAA Degradation Pathways
Liver
Muscle
BAT
Bcat1
Hmgcs1
Ehhadh
Il4i1
Acat1
Hadha
Hadhb
Mccc1
Pcca
Oxct2b
Aldh2
Abat
Aldh9a1
Hmgcl
Hmgcs2
Aox1
Aldh3a2
Acat2
Acadsb
Dbt
Mmut
Pccb
Bcat2
Oxct1
Bckdha
Dld
Aldh1b1
Echs1
Ivd
Bckdhb
Aldh6a1
Hibadh
Mccc2
Hagh
Acaa1a
Hsd17b10
Aldh7a1
Hibch
Acads
Mcee
Acad8
Auh
Acaa2
Acadm
Female
Male
Log₂ Fold Change

Figure 4: Multi-tissue transcriptomic analysis of male and female mice on Val-R.

(A) A principal component analysis (PCA). (B) Top 50 differentially expressed genes (DEGs) in the liver, muscle and adipose tissue. (C) Venn diagram of number of gene changes by tissue in male and female mice. (D) KEGG pathway analysis in liver, muscle and BAT in male and female mice. (E) Altered genes in the BCAA degradation pathway in the liver, muscle and BAT. (A-E) n=6-10 mice/group.

Figure 5

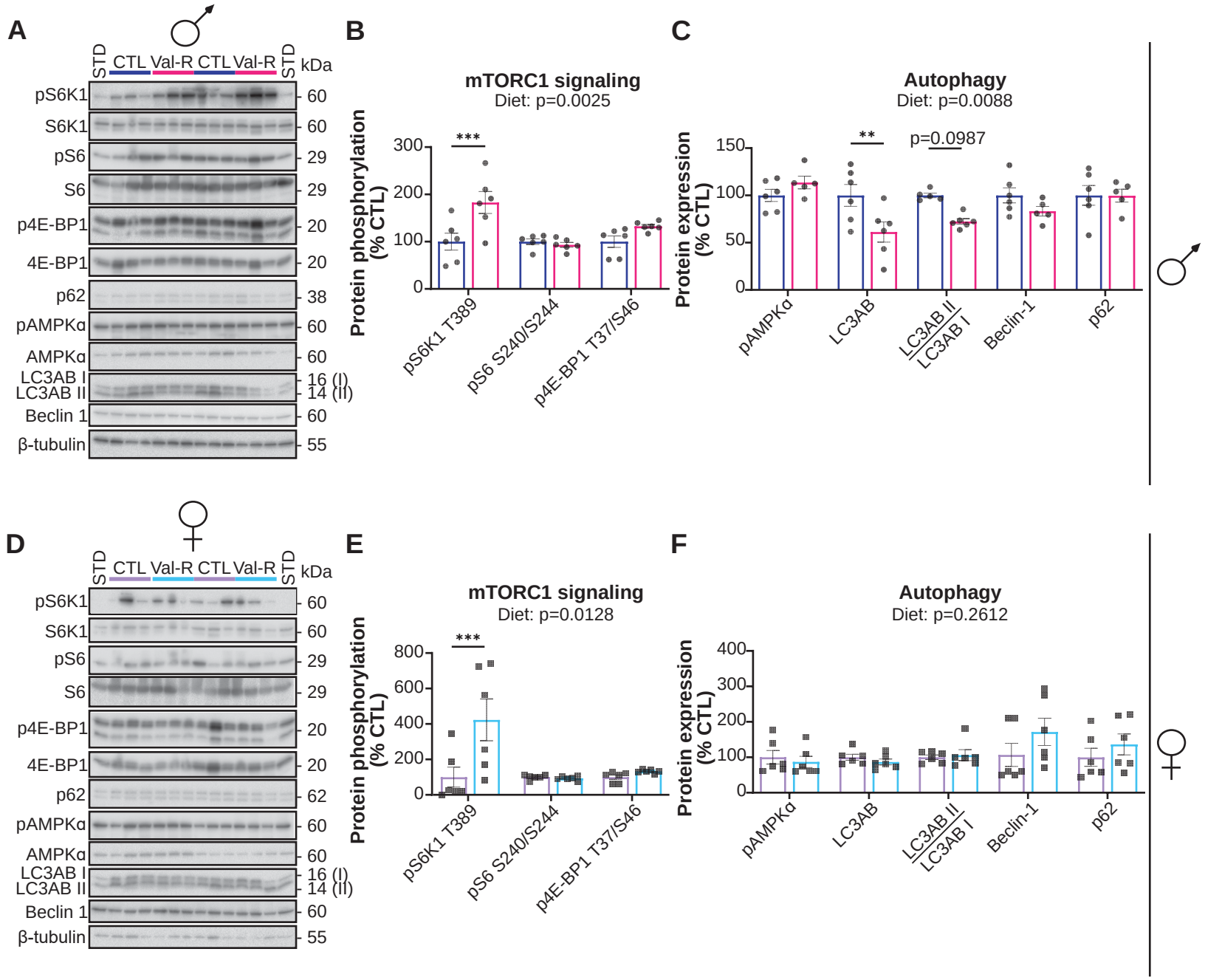
A
STD CTL Val-R CTL Val-R STD kDa
pS6K1 60
S6K1 60
pS6 29
S6 29
p4E-BP1 20
4E-BP1 20
p62 38
pAMPKα 60
AMPKα 60
LC3AB I 16 (I)
LC3AB II 14 (II)
Beclin 1 60
β-tubulin 55
B
mTORC1 signaling
Diet: p=0.0025
Protein phosphorylation (% CTL)
***
pS6K1 T389
pS6 S240/S244
p4E-BP1 T37/S46
C
Autophagy
Diet: p=0.0088
Protein expression (% CTL)
**
p=0.0987
pAMPKα
LC3AB
LC3AB II / LC3AB I
Beclin-1
p62
D
STD CTL Val-R CTL Val-R STD kDa
pS6K1 60
S6K1 60
pS6 29
S6 29
p4E-BP1 20
4E-BP1 20
p62 62
pAMPKα 60
AMPKα 60
LC3AB I 16 (I)
LC3AB II 14 (II)
Beclin 1 60
β-tubulin 55
E
mTORC1 signaling
Diet: p=0.0128
Protein phosphorylation (% CTL)
***
pS6K1 T389
pS6 S240/S244
p4E-BP1 T37/S46
F
Autophagy
Diet: p=0.2612
Protein expression (% CTL)
pAMPKα
LC3AB
LC3AB II / LC3AB I
Beclin-1
p62

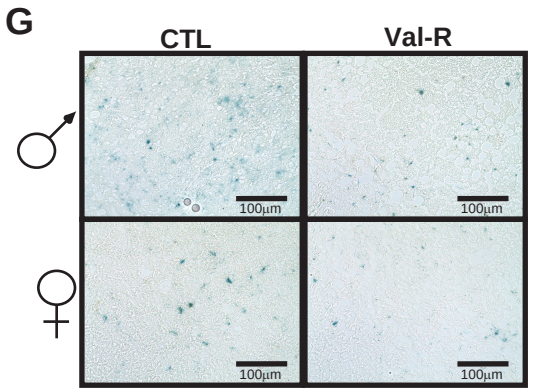
G
CTL
Val-R
100µm

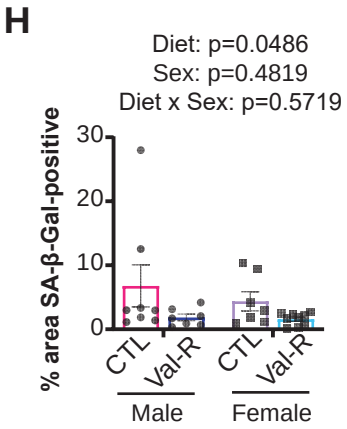
H
Diet: p=0.0486
Sex: p=0.4819
Diet x Sex: p=0.5719
% area SA-β-Gal-positive
CTL
Val-R
Male
Female

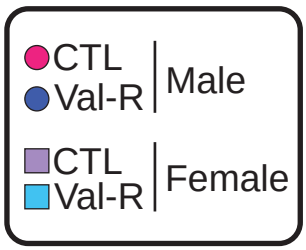
CTL
Val-R
Male
CTL
Val-R
Female

Figure 5: Val-R induced hepatic mTORC1 signaling.

(A) Western blots of the analyzed proteins in male livers. (B) Phosphorylation of S6K1 T389, S6 S240/S244 and 4E-BP1 T37/S46, normalized to the expression of the respective protein. (C) Phosphorylation of AMPKα normalized to the expression of AMPKα and protein expression of LC3AB, Beclin-1 and p62 normalized to expression of β-tubulin (n=5-6 mice/group). (D) Western blots of the analyzed proteins in female livers. (E) Phosphorylation of S6K1 T389, S6 S240/S244 and 4E-BP1 T37/S46 normalized to their total protein. (F) Phosphorylation of AMPKα normalized to the expression of AMPKα and protein expression of LC3AB, Beclin-1 and p62 normalized to expression of β-tubulin (n=6 mice/group). (G-H) Hepatic SA-β-Gal staining at 40X magnification (scale bar = 100 μm) (G) with quantification of SA-βGal-positive cells (H) (n=7-10 mice/group). (B-C, E-F, H) statistics for the overall effects of gene or sex, diet, and the interaction represent the p value from a two-way RM ANOVA analysis; **$p<0.01$, ****$p<0.0001$ from a Sidak's post-test examining the effect of parameters identified as significant in the 2-way ANOVA or student's t-test. Data represented as mean ± SEM.

Figure 6

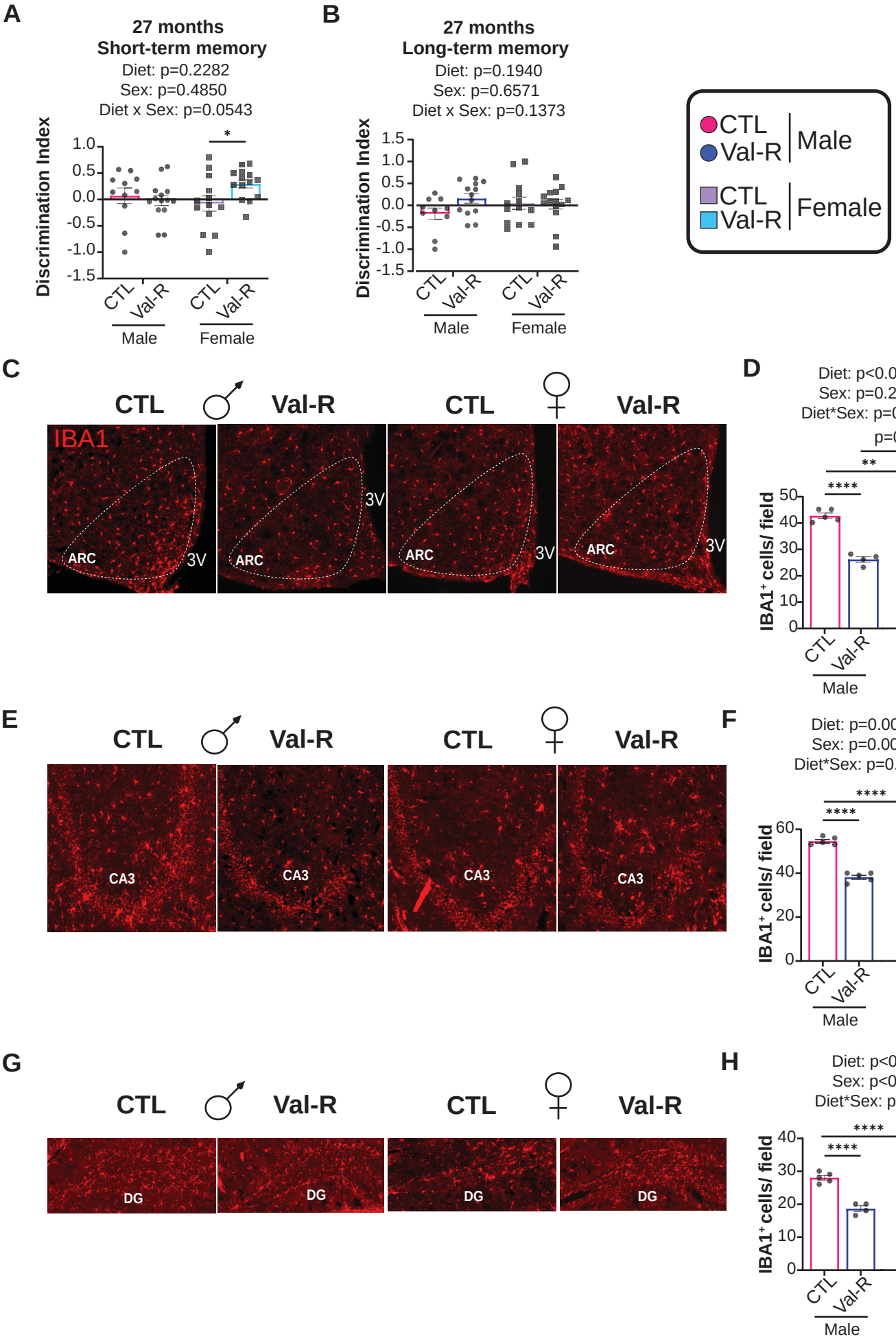
A
27 months
Short-term memory
Diet: p=0.2282
Sex: p=0.4850
Diet x Sex: p=0.0543
Discrimination Index
1.0
0.5
0.0
-0.5
-1.0
-1.5
*
CTL
Val-R
CTL
Val-R
Male
Female
B
27 months
Long-term memory
Diet: p=0.1940
Sex: p=0.6571
Diet x Sex: p=0.1373
Discrimination Index
1.5
1.0
0.5
0.0
-0.5
-1.0
-1.5
CTL
Val-R
CTL
Val-R
Male
Female
CTL
Val-R
Male
CTL
Val-R
Female
C
CTL
Val-R
CTL
Val-R
IBA1
ARC
3V
ARC
3V
ARC
3V
ARC
3V
D
Diet: p<0.0001
Sex: p=0.2844
Diet*Sex: p=0.0011
p=0.0618
**
****
*
IBA1+ cells/ field
50
40
30
20
10
0
CTL
Val-R
CTL
Val-R
Male
Female
E
CTL
Val-R
CTL
Val-R
CA3
CA3
CA3
CA3
F
Diet: p=0.0020
Sex: p=0.0003
Diet*Sex: p=0.0030
****
****
IBA1+ cells/ field
60
40
20
0
CTL
Val-R
CTL
Val-R
Male
Female
G
CTL
Val-R
CTL
Val-R
DG
DG
DG
DG
H
Diet: p<0.0001
Sex: p<0.0001
Diet*Sex: p<0.0001
****
****
IBA1+ cells/ field
40
30
20
10
0
CTL
Val-R
CTL
Val-R
Male
Female

Figure 6: Val-R improves cognition in female mice and reduced neuroinflammation in Val-R-fed males and females.

(A-B) Novel object recognition test discrimination index in the short-term memory test of males and females (A), and the long-term memory test in males and females (B) (n=10-14 mice/group). (C, E, G) Representative images of Iba1 staining in the Arc, CA3 and DG of the brain. (D, F, H) Quantified staining of Iba1 in the Arc (D), CA3 (F) and DG (H) (n=3-6 mice/group). (A-B, D, F, H) statistics for the overall effects of sex, diet, and the interaction represent the p value from a two-way RM ANOVA analysis; *$p<0.05$, **$p<0.01$, ****$p<0.0001$ from a Sidak's post-test examining the effect of parameters identified as significant in the 2-way ANOVA or student's t-test. Data represented as mean ± SEM.

Figure 7

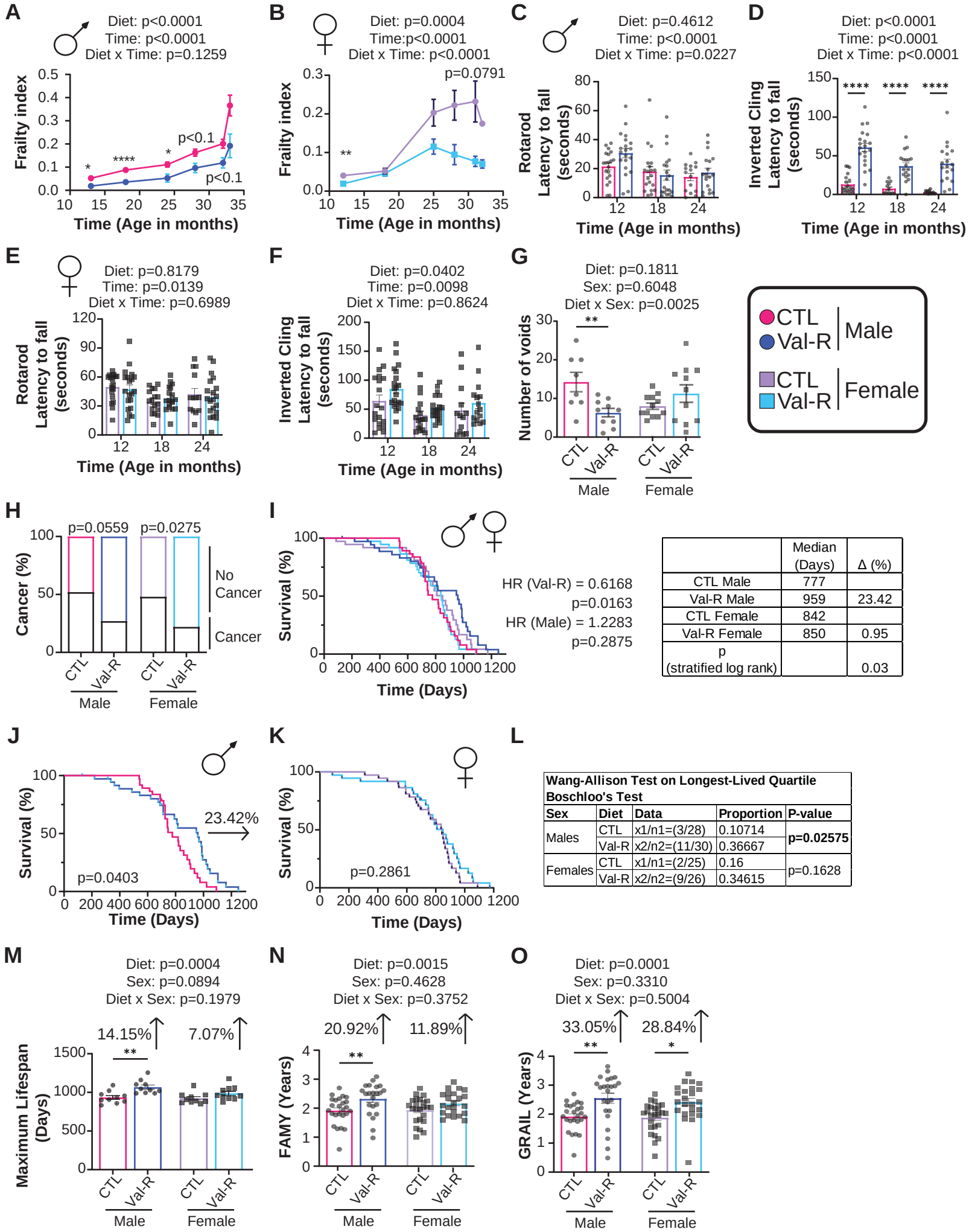

	Median (Days)	Δ (%)
CTL Male	777	
Val-R Male	959	23.42
CTL Female	842	
Val-R Female	850	0.95
p (stratified log rank)		0.03

Wang-Allison Test on Longest-Lived Quartile
Boschloo's Test

Sex	Diet	Data	Proportion	P-value
Males	CTL	x1/n1=(3/28)	0.10714	**p=0.02575**
	Val-R	x2/n2=(11/30)	0.36667	
Females	CTL	x1/n1=(2/25)	0.16	p=0.1628
	Val-R	x2/n2=(9/26)	0.34615	

Figure 7: Val-R improves health of both males and females and extends lifespan in male mice.

(A-B) Frailty index scoring of male (A) and female (B) mice from 12 to 32 months of age in mice. (C) Rotarod latency to fall in seconds at 12, 18 and 24 months of age in male mice (n=25 mice/group). (D) Inverted cling latency to fall in seconds at 12, 18 and 24 months of age in male mice. (E) Rotarod latency to fall in seconds at 12, 18 and 24 months of age in female mice (n=15-20 mice/group). (F) Inverted cling latency to fall in seconds at 12, 18 and 24 months of age in female mice (n=15-20 mice/group). (G) Void spot assay conducted in 27-month-old male and female mice (n=8-12 mice/group). (H) Percent of male and female mice with and without cancer observed at necropsy from lifespan in (I-K). (I) Kaplan-Meier plots showing the survival of male and female (n=37 biologically independent animals for both groups). Table of median lifespans for mice on each diet, percent change between Val-R-fed and Control-fed mice of the same sex, and the two-sided Gehan-Breslow-Wilcoxon p-value between Val-R-fed and CTL-fed mice of the same sex. (J) Kaplan-Meier plots showing the survival of male (n=37 biologically independent animals for each diet). (K) Kaplan-Meier plots showing the survival of female (n=37 biologically independent animals for each diet). (L) Table of maximum lifespan calculations were made by generating a cutoff of the top 25% longest lived animals in each sex, coupled with Boschloo's Test (Wang-Allison) for significance testing between groups. (M) Maximum lifespan of top 10 longest lived mice per group per sex (n=10 mice/group). (N) Frailty-Adjusted Mouse Years (FAMY) in years was calculated using the survival and frailty data plotted in panels A-B and J-K (n=24-25 mice/group). (O) Gauging Robust Aging when Increasing Lifespan (GRAIL) in years calculated using the survival and frailty data plotted in panels A-B and J-K (n=24-25 mice/group). (C-G, M-O) statistics for the overall effects of time or sex, diet, and the interaction represent the p value from a two-way ANOVA analysis; *$p<0.05$, **$p<0.01$, ***$p<0.001$, ****$p<0.0001$ from a Sidak's post-test examining the effect of parameters identified as significant in the 2-way ANOVA. Data represented as mean ± SEM.

Figure 8

A

Module−trait relationships

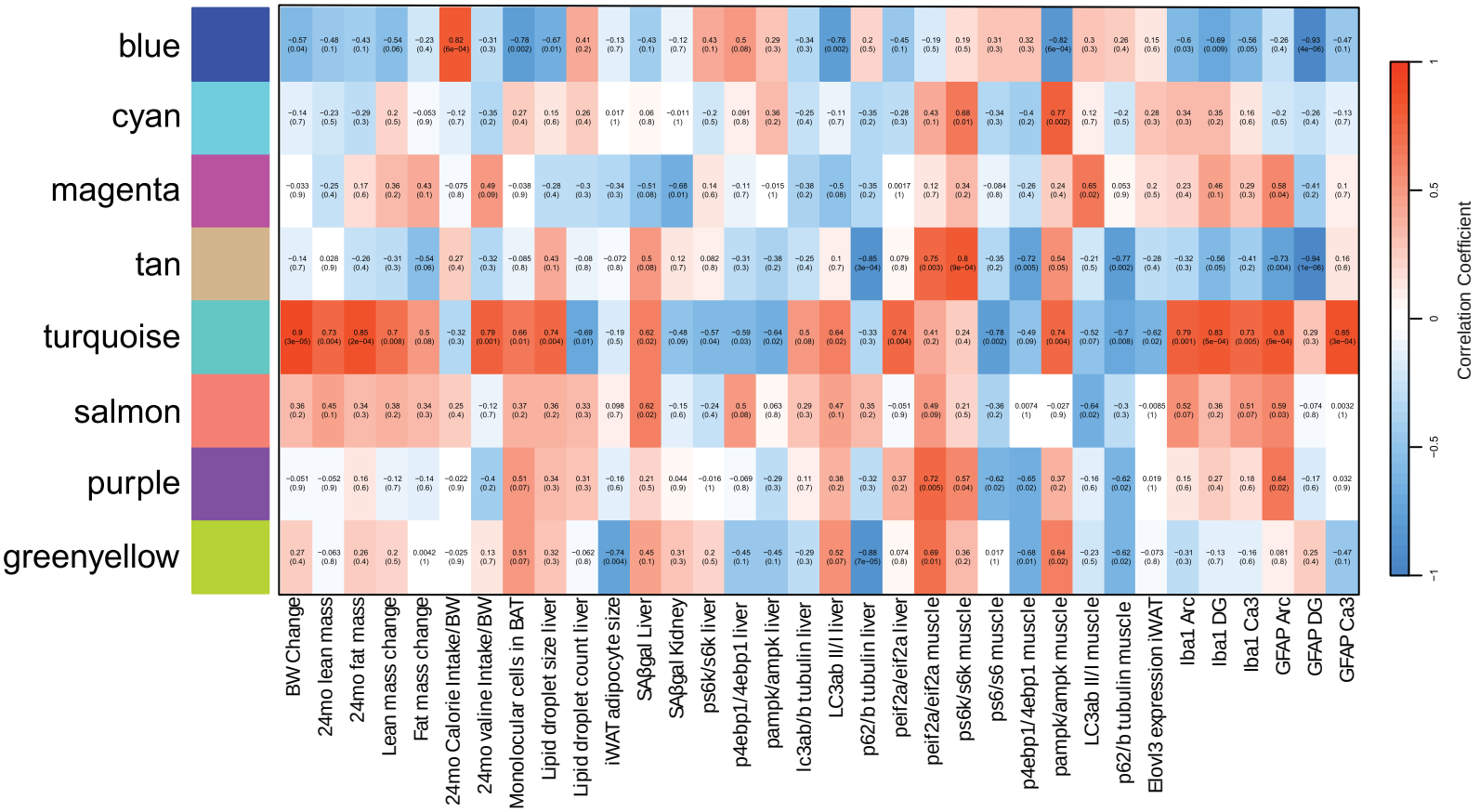

B

Turquoise module pathway enrichment

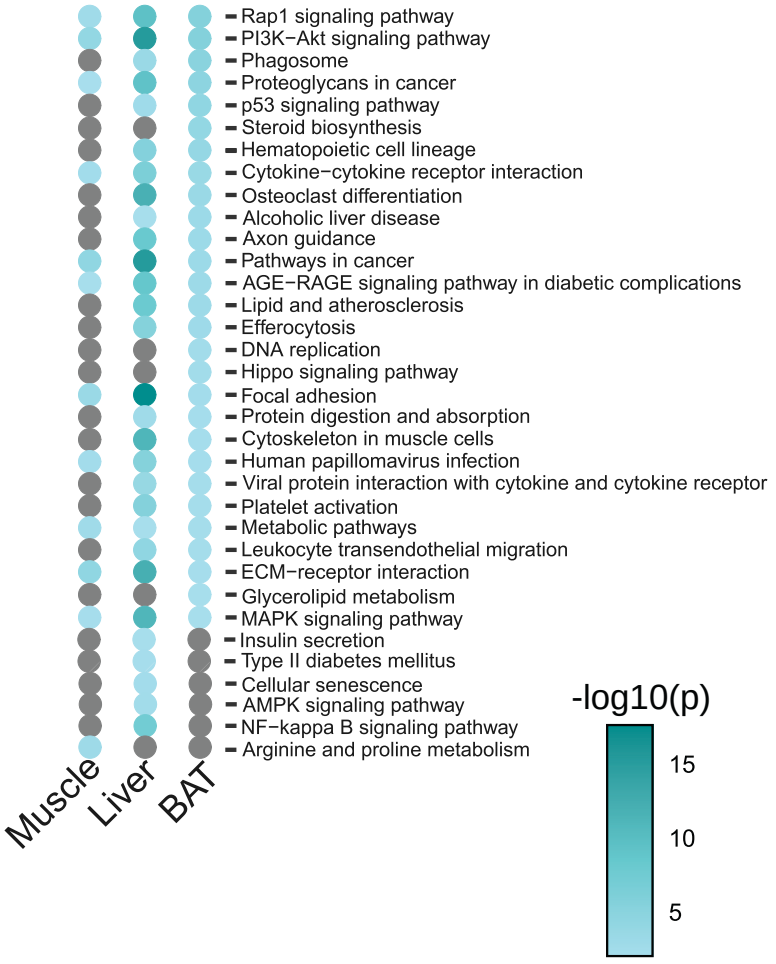

C

PI3K-Akt Signaling Pathway Genes

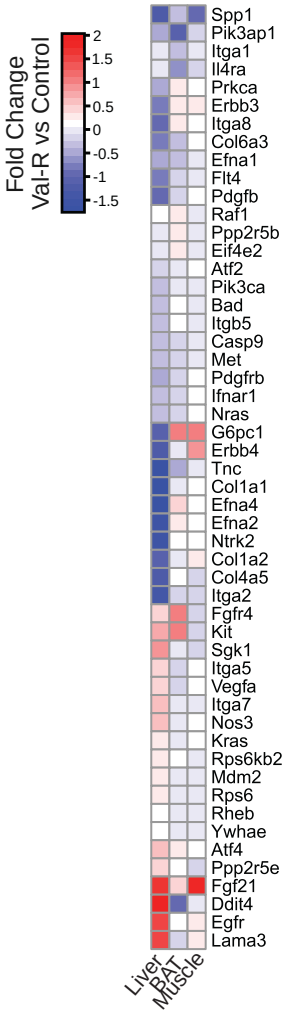

D

MAPK Signaling Pathway Genes

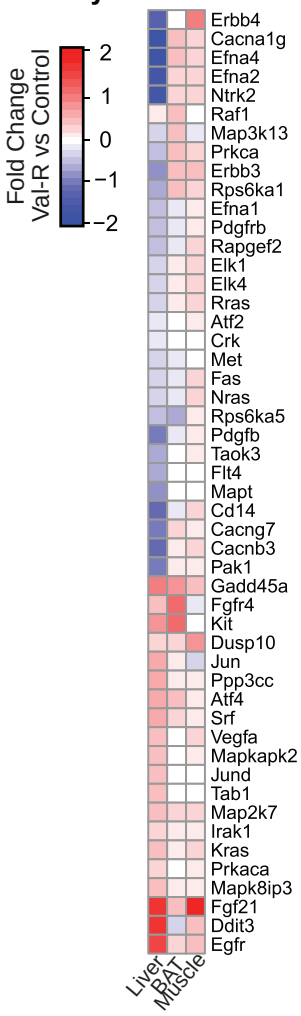

Figure 8: WGCNA analysis of selected modules and pathways in males.

(A) Pearson correlation coefficient between the gene modules and selected phenotypic traits, numbers in brackets indicate the corresponding p values in males (n=6-9 mice/group). (B) Selected KEGG pathway enrichment of turquoise module. Gray dots indicate no alterations in that pathway for that tissue. (C-D) Altered genes in the PI3K-Akt signaling pathway (C) and the MAPK signaling pathway (D) in the liver, muscle and BAT. Genes shown were significantly altered (Benjamini-Hochberg (BH) adjusted $p<0.05$) by Val-R in at least one tissue in males or females.